Alternative Hybrid Empirical Ground-Motion Model for Central and Eastern North America using Hybrid Simulations and NGA-West2 Models

Alireza Shahjouei and Shahram Pezeshk

Abstract

An alternative hybrid empirical ground-motion model for the central and eastern North America (CENA) is proposed. The new ground-motion model (GMM) is developed for the average horizontal components (RotD50) of peak ground acceleration (PGA), peak ground velocity (PGV), and 5%-damped pseudo-spectral accelerations (PSAs) at spectral periods of 0.01–10s. Hybrid empirical estimates are derived using the regional modification factors between two regions (host and target) along with empirical GMMs from the host region. The regional adjustment factors are ratios of the intensity measures from the generated synthetics in the host (western North America, WNA) and target (CENA) regions. In this study, the recent updated empirical GMMs developed by the Pacific Earthquake Engineering Research Center (PEER) for the NGA-West2 project (Bozorgnia et al., 2014) are incorporated. We used a broadband simulation technique proposed by the authors (Shahjouei and Pezeshk, 2015a) to generate synthetics for both the WNA and CENA regions in which the high frequency and low frequency parts of synthetics are calculated through a stochastic finite-fault method and kinematic source models along with the deterministic wave propagation, respectively. The updated seismological and geological parameters are incorporated in simulations.

The new ground-motion model is developed, as part of the NGA-East research project, considering multiple shaking scenarios which characterize the magnitude in the range of **M**5.0–8.0. The proposed GMM represents the level of ground shaking in the distance range of 2–1000

km and are developed for the reference rock site condition with V_{s30} = 3 km/s in CENA. The results are compared with some other existing models in the region. In addition, a comprehensive residual analysis is performed using the recorded earthquakes available in the NGA-East database.

Introduction

Ground-motion prediction equations or ground-motion models (GMMs) provide the expected level of shaking in terms of ground-motion intensity measures as a function of earthquake magnitude, site-to-source distance, and local site parameters (and sometimes also as a function of style of faulting mechanism and other parameters). Such ground-motion models are used in seismic hazard and risk applications as well as site-specific engineering studies (Kramer, 1996; Bozorgnia and Campbell, 2004; Stirling, 2014). The intensity measures or parameters mostly referred to as the peak ground motions include peak ground acceleration (PGA), peak ground velocity (PGV), and damped pseudo-absolute response spectral accelerations (PSAs), usually 5%-damped PSAs. In active crustal regions with high seismicity where strong ground motions are well recorded, such as the active tectonic area of western North America (WNA), GMMs are empirically developed from the recorded earthquakes by applying empirical regressions of observed amplitudes against predictor variables (Douglas, 2003; 2011). On the other hand, for regions with the historical seismicity but deficient recorded strong ground motions such as central and eastern North America (CENA), GMMs are theoretically or semi-empirically constructed (Campbell, 2003; Bozorgnia and Campbell, 2004; Pezeshk et al., 2011).

Recent empirical ground-motion models (EGMMs) in active crustal regions include Abrahamson et al. (2014), Boore et al. (2014), Campbell and Bozorgnia (2014), Chiou and Youngs (2014), and Idriss (2014) relations developed as part of the Next Generation Attenuation project (i.e., NGA-West2) by the Pacific Earthquake Engineering Research Center (PEER) (Bozorgnia et al., 2014).

In regions where there are demands for engineering and/or seismological applications but lack of strong recorded ground motions, generation of the synthetic earthquake time series is a promising solution (Ghodrati et al., 2011; Pezeshk et al., 2011). The stochastic method is a simulation approach commonly used by engineers and seismologists to generate strong ground motions for the desired earthquake magnitude and distance utilizing the seismological model in a simple yet powerful manner (Boore 1983; 2003; Hanks and McGuire, 1981). The point-source stochastic method predicts the ground motions by considering a random process over almost all frequencies, so it is deficient in capturing the inherent near-source characteristics (particularly in the long period portion) that are usually observed in the recorded data. This deficiency is improved by applying the stochastic double corner frequency model (Atkinson and Silva, 1997; Atkinson and Boore, 1998) and, more effectively, by using the finite-fault stochastic model (Beresnev and Atkinson, 2002; Motazedian and Atkinson, 2005; Atkinson and Boore, 2006).

The hybrid broadband (HBB) simulation method is another earthquake simulation technique in which broadband synthetics for the entire frequency band of interest are developed by combining deterministically-generated long-period synthetics with high-frequency synthetics. Recent technological developments in high performance computing enables researchers to utilize and extend the implementation of broadband simulation techniques in broader applications. Examples of broadband models are proposed and incorporated by Zeng et al. (1994), Hartzell et al. (2005), Liu et al. (2006), Frankel (2009), Graves and Pitarka (2004; 2010), Mai et al. (2010), Mena et al. (2010), Olsen (2012), and Shahjouei and Pezeshk (2015a). Summaries of validation of ground-motion simulation methods used on the Southern California Earthquake Center (SCEC) Broadband Platform (BBP)—an open-source software for the physic-based ground-motion simulation—are recently presented by studies of Anderson (2015), Atkinson and Assatourians (2015), Crempien and Archuleta (2015), Douglas et al. (2015), Goulet et al. (2015), Graves and Pitarka (2015), and Olsen and Takedatsu (2015).

As discussed earlier, synthetic seismograms are implemented to develop GMMs for CENA in the absence of sufficient appropriately recorded strong ground motions. A number of ground-motion relations are currently available and are used in this region: the stochastic-based, hybrid empirical-based, reference empirical-based, and full wave-based (or numerical-based) models. Frankel et al. (1996), Toro et al. (1997), Toro (2002), and Silva et al. (2002) developed GMMs using the stochastic method (with single corner frequency). Ground-motion relations developed by Atkinson and Boore (2006, 2011) incorporated the stochastic finite-fault simulations (with dynamic corner frequency). Campbell (2003; 2007), Tavakoli and Pezeshk (2005), and Pezeshk et al. (2011) proposed hybrid-empirical GMMs for eastern North America (ENA). Pezeshk et al. (2015) updated their model using the new sets of parameters as part of the NGA-East project. Atkinson (2008) suggested a reference empirical model based on regional ground-motion observations in ENA. Later on, she revised her model in light of new data and presented it in Atkinson and Boore (2011). A full waveform simulation technique is used by Somerville et al. (2001; 2009) to develop GMMs.

For the central and eastern U.S. (CEUS), the 2014 update of the USGS National Seismic Hazard Maps (NSHMs) published by the U.S. Geological Survey (i.e., 2014 USGS NSHMs) incorporated the following ground-motion relations: Frankel et al. (1996), Toro et al. (1997), Toro (2002), Silva et al. (2002), Atkinson and Boore (2006; 2011), Campbell (2003), Tavakoli and Pezeshk (2005), Pezeshk et al. (2011), Somerville et al. (2001), and Atkinson and Boore (2011) through a logic tree process by assigning different weights to each model. The weights are assigned based on parameters such as the model type, applicability of the model over the distance range, etc. (Petersen et al., 2014).

This study proposes an alternative hybrid empirical GMM for CENA by implementing the hybrid broadband simulation technique and using the recent proposed empirical NGA-West2 GMMs (Abrahamson et al., 2014; Boore et al., 2014; Campbell and Bozorgnia, 2014; Chiou and Young, 2014; Idriss, 2014). Synthetics are generated for both host (WNA) and target (CENA) regions using the hybrid broadband simulation approach recently proposed by the authors (Shahjouei and Pezeshk, 2015). In this study, the recent updated and suggested geological and seismological parameters in the synthetic simulations are incorporated. The model is developed for the moment magnitudes (**M**) in the range of 5–8, and for the Joyner-Boore distances (R_{JB}: horizontal distance to the surface projection of the rupture plane) in the range of 2–1000 km. The new model provides PGA (g), PGV (cm/s), and 5%-damped PSA (g) in the spectral period range of 0.01–10s for a generic hard rock site condition with shear velocity of 3000 m/s in CENA (Hashash et al., 2014). The proposed model is compared with the available GMMs and validated with the recorded data in the region. The median GMM is recently published in the PEER report as part of the NGA-East multidisciplinary research project (chapter 7 by Shahjouei and Pezeshk, 2015b). This study is updating Shahjouei and Pezeshk (2015b) by considering additional earthquake simulations using the most recent seismological parameters. The refined median GMMs as well as the aleatory variability and epistemic uncertainty model are presented in this manuscript.

Review of Hybrid Empirical Method

The hybrid empirical method (HEM) is a powerful technique to develop GMMs in regions with a shortage of recorded strong ground motions. The procedure was first proposed by Campbell (1981) to estimate ground motions in ENA. The idea also was implemented by Nuttli and Herrmann (1984) to develop ground-motion models in the Mississippi Valley. Abrahamson and Silva (2001) and Atkinson (2001) afterward used the HEM technique in ENA. Campbell (2003) provided a comprehensive mathematical framework for HEM and developed the GMM for this region. Tavakoli and Pezeshk (2005) applied the HEM technique and proposed ground-motion models for ENA using stochastic simulations. Later, Pezeshk et al. (2011) revised their previous models using the updated seismological parameters and empirical ground-motion models provided in the NGA-West1 project (Power et al., 2008). A complete review and evaluation of ground-motion relations that applied the HEM technique for ENA was presented by Campbell (2014).

Framework

HEM derives the ground-motion model for the desired region (target) based on some modifications on the empirical ground-motion models which have already been developed in the well-recorded earthquake area (host). The modification is performed using the regional adjustment factors which are the ratios of the intensity measures of ground motions between two regions.

In this study, WNA is selected as the host because there are well constrained empirical GMMs available to use for this region. Furthermore, seismological models used in synthetic simulations which represent the earthquake source, wave propagation, site condition, and crustal structure models exist for both the target (ENA) and host (WNA) regions. The regional modifications implemented in HEM account for the differences in seismological models such as source scaling and wave propagation used in synthetic simulations (Campbell, 2007; Pezeshk et al., 2011).

The broadband synthetics for the two regions are calculated using the HBB simulation technique. The applied model parameters will be described and presented in the following section. By applying adjustment factors the hybrid empirical estimates of ground motions are calculated and are then used to develop GMMs for CENA.

Ground-Motion Simulations

In the previous applications of HEM, Tavakoli and Pezeshk (2005), Campbell (2003; 2007) and Pezeshk et al. (2011) used the stochastic method in synthetic simulations. Shahjouei and Pezeshk (2015a) generated broadband synthetics for CENA using a hybrid broadband simulation technique. In this study, we have extended the application of the procedure to develop broadband synthetics for both CENA and WNA to be applied in HEM. In the broadband procedure, the low-frequency (LF) portion of synthetics is obtained through a deterministic approach, implementing kinematic source models and the discrete wavenumber-finite element method for wave propagation using the program COMPSYN (Spudich and Xu, 2003). The high-frequency (HF) portions are derived from a finite-fault stochastic simulation where the heterogeneous stress distribution over the fault is used. We have implemented the stochastic approach of the SMSIM program (Boore, 2012) to obtain the HF part of the synthetics. These stochastic synthetics are summed up over the fault plane, scaled with the magnitude, and then combined with the long-period traces using matched filters. The flowchart of the procedure along with the detailed information were described in Shahjouei and Pezeshk (2015a). To compute intensity measures, two components of the broadband synthetics at each station generated from each shaking scenario are rotated and the RotD50 intensity parameters of broadband synthetics are computed. The RotD50 is an alternative designation of the mean horizontal component that is orientation-independent, while spectral period-dependent. In other words, it is a single component across all non-redundant azimuths (Boore, 2010). The RotD50 intensities are calculated using the package provided by David Boore in his website (Boore, 2010; Boore et al., 2006).

To consider uncertainties associated with applying different parameters, at any given magnitude of **M**5.0, 5.5, 6.0, 6.5, 7.0, 7.5, and 8.0, we have defined 9 and 18 source representations of strike slip faulting mechanisms for WNA and CENA, respectively. The variability includes the hypocenter locations, distributions of slip, stress, rise time, slip velocity, and rupture propagation over the fault plane. Other faulting mechanisms such as reverse faulting with shallower dips will be considered in future studies. The ground-motion intensity measures are obtained from synthetic time histories generated from 63 (9×7) and 126 (18×7) earthquake source models in WNA and CENA, respectively. The source models respectively represented 9 and 18 shaking scenarios used for each of 7 earthquake magnitude simulations. These synthetics are calculated at stations with a distance range of 2–1000 km distributed with different azimuths.

Long Period Simulation Parameters

The LF synthetics are calculated based on the mathematical framework of the discrete wavenumber-finite element technique provided in the COMPSYN package (Spudich and Xu, 2003) which has been widely used in the literature. The software package generates the low-frequency Green's function based on the predefined kinematic source characteristics. Shahjouei and Pezeshk (2015a) represented several examples of kinematic source models in which distributions of the slip, rise time, slip velocity, and stress over the finite-fault plane as well as the rupture front are represented. A kinematic source representation used in this study is discussed next.

Rupture areas

There are few empirical equations that provide an estimate of the faulting areas and dimensions. Such relations are derived either from the indirect earthquake measurement (e.g., rupture length) as proposed by Wells and Coppersmith (1994), Working Group on California Earthquake Probabilities (WGCEP, 2003), and Hanks and Bakun (2002), or from the direct earthquake measurement (e.g., seismic radiation) as proposed by Somerville et al. (1999), Mai and Beroza (2000), and Somerville (2006).

We employed the average results from the abovementioned models to calculate fault dimensions in the WNA as a tectonically active area. Somerville et al. (2001; 2009) suggested using smaller rupture areas for stable continental regions like CENA (as compared to active tectonic regions), which is also considered in the source modeling of CENA in this study. A summary of the fault geometry and rupture areas used in this study is provided in Table 1. Table 1 includes the length and width fault, the depth ranges applied to the top of ruptures and hypocenter locations for all magnitude simulations. The parameters are consistent with the suggested and applied values from the other studies in the NGA-East project (e.g., Frankel, 2015).

Slip, rise time, and slip rate distributions

The estimated average slip for a given magnitude and faulting area is distributed over the fault plane assuming a wavenumber-squared spectral decay, k^{-2} (Graves and Pitarka, 2010). The heterogeneous slip distribution is constructed using the von Karman auto correlation function (ACF) suggested by Mai and Beroza (2002) as a spatial random field model. Rupture initiated at a hypothetical location is propagated over the fault plane following the proposed approach by Graves and Pitarka (2010). A depth-dependent rupture velocity is used in the procedure. The rupture front in this approach is calculated as a function of the local, maximum, and average of slip over the fault plane as well as the seismic moment.

The slip velocity is calculated using source time functions (STF) and the rise time parameter. The simulations are performed using different STFs in different simulations. Examples of STFs are boxcar, exponential, and Regularized Yoffe (Tinti et al., 2005; Liu et al., 2006). In this study, the average rise time parameter for CENA and WNA are calculated using the magnitude-dependent relations proposed by Somerville et al. (1999; 2001; 2006; 2009) and the dip-dependent modification suggested by Graves and Pitarka (2010). The rise time is also heterogeneously distributed over the fault area implementing the approach suggested by Graves and Pitarka (2010). This local slip-dependent and depth-dependent distribution approach accounts for the trade-off between assuming a constant slip velocity and a constant rise time. A summary of some of the source parameters in our simulations is provided in Table 2.

Hypocenter location and seismogenic zone

Usually the earthquake's depths are distributed in the range of 3–15 km. The upper depth of the seismogenic zone, or depth of the top of rupture, Z_{TOR}, is a controversial topic (Stanislavsky and Garven, 2002). Atkinson and Boore (2011) used a magnitude-dependent equation $(Z_{TOR} = 21. - 2.5\mathbf{M})$ to estimate Z_{TOR}. Frankel (2009) applied a 3 km depth in simulations for all magnitudes for WNA. Simulations of **M**7.4–7.7 New Madrid Seismic Zone (NMSZ) events are performed using 1 km as the minimum depth of rupture in the study of Olsen (2012). Following the previous discussion and to be consistent with observations of CEUS Seismic Source Characterization as part of the NGA-East project, we implemented a magnitude-dependent depth of 2–5 km and 1–4 km as Z_{TOR} for **M**8–5, in CENA and WNA, respectively.

Atkinson and Silva (2001) used a magnitude dependent relation ($\log_{10} h = -0.05 + 0.15\mathbf{M}$) to estimate the hypocenter depth to be incorporated in the point-source stochastic simulations. The relation was revised to $\log_{10} h = \max(-0.05 + 0.15\mathbf{M}, -1.72 + 0.43\mathbf{M})$ in the study of Yenier and Atkinson (2014). Other magnitude-dependent relations to estimate the hypocenter depth are proposed by Scherbaum et al. (2004) for different styles of fault mechanism ($Z_{Hyp} = 5.63 + 0.68\mathbf{M}$ for strike slip and $Z_{Hyp} = 11.24 - 0.2\mathbf{M}$ for non-strike slip). Mai et al. (2005) suggested the hypocenter depth for crustal dip-slip earthquakes to be about the lower 60% of the rupture depth. Based on the abovementioned recommendations, the hypocenter depth in our study varies in each shaking scenario by about 0.5–0.8 of the fault width. We have considered three hypothetical rupture initiation points (hypocenters) along the strike of the fault (L) as L/4–L/3, L/2, and 2L/3–3L/4. For each hypocenter location, three slip distributions are assigned; therefore, a total of nine shaking scenarios are defined for each magnitude.

Figure 1 shows examples of different kinematic source models used for **M**7 simulations in CENA. The variability of slip distribution, rupture front, and hypocenter location in simulations is sampled in this figure to account for uncertainties associated with the source parameters.

High Frequency Simulation Parameters

High frequency synthetics are calculated using stochastic finite-fault simulations. The synthetics at each sub-fault are calculated through the stochastic method using the software package SMSIM (Boore, 2012). The stochastic synthetics at each station are computed by summing up the sub-fault stochastic synthetics over the fault plane (considering the appropriate delays accounted for by their arrival times) followed by convolving with a source time function using the Frankel (1995) approach. The stochastic point-source simulation at each sub-fault is developed using a different initial seed number.

The point-source stochastic simulations at each sub-fault are incorporated in the following equation proposed by Boore (2003) to derive the displacement Fourier amplitude spectrum $Y(M_0, R, f)$. The spectral amplitude includes different terms of the point-source $E(M_0, f)$, path effect $P(R, f)$, local site response effect $G(f)$, and the type of ground motion $I(f)$.

$$Y(M_0, R, f) = E(M_0, f)P(R, f)G(f)I(f) \tag{1}$$

in which R (km) is the distance, M_0 (dyn.cm) is the seismic moment, and f is the frequency.

The stochastic parameters used in the high-frequency simulations for the CENA and WNA regions are given in Table 3. To consider uncertainties associated with the variability of parameters, two sets of parameters suggested and used by investigators are employed in CENA and are equally weighted to obtain the final results. A new proposed set of parameters for the WNA region is used.

Earthquake source term

The Brune ω-square source spectrum as a single corner frequency source spectrum is used in this study for both the host and target regions. The key element in this source model is the stress-drop parameter ($\Delta\sigma$), which controls the amplitude of spectrum at high frequencies.

The finite-fault simulations at each sub-fault are performed using a local stress-drop parameter assigned at each point on the fault. The correlation between the stress and slip distribution used in HF and LF simulations, respectively, are taken into account. In this study, we used the stress distribution procedure proposed by Ripperger and Mai (2004) and Andrews (1980) in simulations. This technique correlates the local slip to the local stress at a given point over the fault plane. The final stress distribution is achieved by applying a scaling factor to match the geometric mean of the stress over the fault to the desired values given in Table 3.

Campbell (2003) and Tavakoli and Pezeshk (2005) used 5 stress parameters in ENA in the range of 105–215 bars with different assigned weights to each one. Atkinson and Boore (2006) applied $\Delta\sigma = 140$ bars in finite-fault stochastic simulations using the EXSIM package by Motazedian and Atkinson (2005). Further studies by Atkinson et al. (2009) and Boore (2009) suggested $\Delta\sigma = 250$ bars in ENA based on observations from the recorded data. Pezeshk et al. (2011) used $\Delta\sigma = 250$ bars in their HEM simulations for ENA. Recently, Atkinson and Boore (2014) suggested the stress term of 600 bars for $\mathbf{M} > 4.5$. Boore and Thompson (2015) applied $\Delta\sigma = 400$ bars compatible with their new path duration model in their stochastic simulations in ENA. Following the discussion, we used stress parameters of 600 bars and 400 bars in the two alternative models for CENA.

In WNA, Campbell (2003; 2007) used 100 bars stress parameters in his HEM model. Atkinson and Silva (2000) suggested $\Delta\sigma = 80$ bars for a single corner frequency source model which also was implemented by Pezeshk et al. (2011). Zandieh et al. (2015) suggest the seismological parameters for WNA based on the inversion of NGA-West2 ground-motion models and they obtained stress parameter of 135 bars for WNA which has also been used in the WNA simulations of this study.

Path effects

The path term takes into account two effects of geometrical spreading, *Z(R)* and anelastic attenuation (known as quality factor, *Q*). One important note is that the selection of the stress parameter is correlated with the geometrical spreading implemented in the model (Boore et al., 2010). Simulations in Atkinson and Boore (2006) were performed using a trilinear geometrical spreading as R^b where b is –1.3, +0.2, and –0.5 for $R < 70$ km, $70 < R < 140$ km, and $R > 140$ km, respectively. They used the quality factor of $Q = 893f^{0.32}$ (with the minimum value of 1000) as the anelastic attenuation following Atkinson (2004). The similar parameters are incorporated in the study of Pezeshk et al. (2011) for simulations in ENA. Atkinson and Boore (2014) suggested the bilinear geometrical spreading with different attenuation rates for distances beyond 50 km (i.e., $R^{-1.3}$ for $R < 50$ km and $R^{-0.5}$ for $R > 50$ km). In addition, they proposed the quality factor of $Q = 525f^{0.45}$ compatible with updated parameters for stochastic simulations. Chapman et al. (2014) developed a tri-linear path duration based on the inversion of broadband data from the EarthScope Transportable Array as $R^{-1.3}$ for $R < 60$ km, R^0 for $60 < R < 120$ km, and $R^{-0.5}$ for $R > 120$ km with the consistent quality factor of $Q = 440f^{0.47}$ for ENA. Following the previous discussion and to be consistent with implementing the other source parameters applied, we employed two alternative sets of geometrical spreading and quality factor relations in CENA simulations of this study.

Campbell (2003) used a bilinear geometrical spreading (i.e., $R^{-1.0}$ for R < 40 km and $R^{-0.5}$ for R > 40 km) and the anelastic attenuation of $Q = 180f^{0.45}$ in simulations of WNA. The parameters originally derived in the study by Raoof et al. (1999) were based on the evaluation of about 180 earthquakes in Southern California. These parameters were supported by further studies by Malagnini et al. (2007) by considering a larger earthquake dataset. Pezeshk et al. (2011) employed the similar path term relations in their study. Zandieh et al. (2015) proposed a tri-linear geometrical spreading model as $R^{-1.03}$ for R < 45 km, $R^{-0.96}$ for 45 < R < 125 km, and $R^{-0.5}$ for R > 125 km consistent with the anelastic attenuation of $Q = 202f^{0.54}$ for WNA. In this study, an anelastic attenuation and geometric spreading function recently proposed by Zandieh et al. (2015) are employed for WNA simulations.

Ground-motion duration consist of the source duration (T_S) and path duration (T_P). Herrmann (1985) suggested a simple path duration ($T_P = 0.05R$) which has been widely used in the literature for WNA (e.g., Atkinson and Silva, 2000; Campbell, 2003; 2007, and Pezeshk et al., 2011). A quadri-linear model of path duration was used by Campbell (2003; 2007) and Pezeshk et al. 2011) for ENA. Boore and Thompson (2014; 2015) proposed a longer path duration for the both WNA and ENA regions which was used in our alternative simulations.

Site effects

The local site effects incorporated two terms of amplification factor, *A(f)*, which is the amplification relative to the source, and a near surface attenuation which represents the loss of energy in high frequencies as a path-independent function (Boore, 2003). This attenuation could be applied through a low-pass filter characterized by the decay parameter of k_0, which has significant effects on the high-frequency slope of spectrum (Boore, 1983).

ENA simulations in the studies of Campbell (2003) and Tavakoli and Pezeshk (2005) were performed using site amplification factors proposed by Boore and Joyner (1997) for the hard-rock site condition with V_{s30} = 2900 m/s. They considered variability in the k_0 (0.012, 0.003, and 0.006 in their models). Campbell (2007) generated synthetics in ENA for the National Earthquake Hazards Reduction Program (NEHRP) B/C site condition with V_{s30} = 760 m/s. He used site amplification factors derived by Atkinson and Boore (2006) for this site condition along with

k_0 = 0.02. Siddiqqi and Atkinson (2002) derived empirical amplification factors for hard-rock site conditions with $V_{s30} \geq 2000$ m/s (NEHRP site class A). These factors along with k_0 = 0.005 were implemented in the ENA simulations of Atkinson and Boore (2006) and Pezeshk et al. (2011). Recently, Hashash et al. (2014) proposed the shear wave velocity of 3000 m/s and the compatible kappa (k_0 = 0.006) as the reference rock site condition for CENA. The V_{s30} = 3 km/s has been derived by applying the quarter-wavelength theory, and by using the data recorded at the geographic regions of the Atlantic coast, the Appalachian Mountains, and the continental interior (the Gulf Coast region was not included) in their study. Atkinson and Boore (2014) set k_0 = 0.005 along with their proposed new Q factor for ENA. Boore and Thompson (2015) revised the Boore and Joyner (1997) site amplification factors and provided a new set of amplification factors for the generic hard rock site condition with V_{s30} = 3000 m/s for CENA. In this study, we used k_0 = 0.005 and 0.006 in our alternative simulations for CENA. The site amplification factors suggested by Boore and Thompson (2015) and Atkinson and Boore (2006) are used to account for V_{s30} = 3 km/s. Currently, the NGA-East working group is investigating to suggest more accurate and reliable site amplification factors corresponding to V_{s30} = 3 km/s.

In WNA, Boore and Joyner (1997) suggested site amplification factors for a rock site condition derived from the quarter-wavelength method. These factors have been used in the WNA simulations by Atkinson and Silva (2000), Campbell (2003; 2007), Tavakoli and Pezeshk (2005), and Pezeshk et al. (2011). A modification to these amplification factors have been provided by Boore and Thompson (2015) for the generic rock site in WNA with V_{s30} = 760 m/s and was used in this study. Anderson and Hough (1984) suggested the average kappa parameter for WNA is in the range of 0.02–0.04 seconds for the hard rock site condition. Atkinson and Silva (1997), Campbell (2003; 2007), Pezeshk et al. (2011), and Al Atik et al. (2014) utilized k_0 = 0.04s in WNA simulations considering compatibility with the other parameters. Zandieh et al. (2015) obtained a kappa value of 0.035 seconds from their inversions, and that has been employed in this study for WNA simulations.

Hybrid Broadband

The HF stochastic and LF synthetics constructed through the abovementioned procedures are combined and filtered to make broadband synthetics. The synthetics are filtered by passing through the matched second-order low-pass and high-pass Butterworth filters. In this study, a magnitude-dependent transition frequency (f_{cross}) between high-frequency and low-frequency synthetics was applied as proposed by Frankel (2009) for **M**5.5, 6.5, and 7.5. We set f_{cross} for **M**5 and 8 to be the same as for **M**5.5, and 7.5, respectively (i.e., 0.8 Hz for **M**7.5 and 8, 3.0 Hz for **M**5 and 5.5) and the f_{cross} for **M**6 and 7 are calculated from interpolation.

Due to extensive computational efforts associated with the generation of deterministic long period synthetics at far distances, the broadband synthetics are computed for near-fault stations with R_{JB} distance of less than 200 km. Those are supplemented with synthetics generated for stations beyond 200 km through the stochastic finite-fault simulations. The similar kinematic stress distribution over the faults which were defined at each shaking scenario and were used for stations closer to the fault was employed for stations at far distances (Shahjouei and Pezeshk, 2015a).

Synthetics were generated considering 126 kinematic source models for CENA and 63 source models for WNA. Seismograms were calculated at 490–670 (varies with magnitude) stations distributed in distances (2–1000 km) and azimuths (0–180°). The numbers of stations are listed in Table 4. For a given shaking scenario and a given station from 2–1000 km, two components of synthetics were rotated using the TSPP (time series processing programs) software package by Boore (2010), and the RotD50 intensity measures were calculated. The high performance computing at the University of Memphis Penguin Computing Cluster Servers is employed to perform the extensive computations.

The crustal structure used in WNA and CENA are given in Table 5 and Table 6, respectively. We used the continent velocity model suggested by Mooney et al. (2012) and Mooney (2013, personal communication) for CEUS. In WNA, the crustal structure used by Frankel (2009) which represents a mean for the western U.S. is implemented in this study. The top layers of crustal structures are modified to represent the reference rock site conditions in both regions.

Empirical Ground-Motion Models in WNA

One of the key elements of the HEM technique is applying appropriate empirical ground-motion models developed for the host region. Pezeshk et al. (2011) incorporated the GMMs from the PEER NGA-West1 project (Power et al., 2008) as empirical ground-motion models for WNA in their HEM model. Recently, the NGA-West1 model developers updated their GMMs as part of the NGA-West2 project (Bozorgnia et al., 2014) in light of additional data available in the NGA-West2 database. This database includes well-recorded shallow crustal earthquakes that occurred worldwide (small-magnitude data from the California region and moderate-to-large data from similar tectonically active regions in worldwide recordings).

We used the following proposed 5 NGA-West2 GMMs in this study for WNA: (1) Abrahamson et al. (2014), (2) Boore et al. (2014), (3) Campbell and Bozorgnia (2014), (4) Chiou and Youngs (2014), and (5) Idriss (2014) models which hereafter are referred to as ASK14, BSSA14, CB14, CY14, and I14, respectively. The weighted geometric mean of the abovementioned GMMs is computed to represent the median empirical ground motion in WNA. The same weights used in the 2014 update of the U.S. national seismic hazard maps (NSHMs) (Petersen et al., 2014) are assigned to each NGA-West2 GMM in this study. The weights are distributed evenly between all GMMs except for I14, which gets one-half as much weight as the others.

The intensity measures in NGA-West2 GMMs are computed using RotD50 parameters, unlike GMRotI50 (the period-independent geometric mean of two horizontal motions) used in the NGA-West1 project. The RotD50 is an alternative designation of the mean horizontal component that is independent of sensor orientation, but in contrast to GMRotI50, is spectral period-dependent (Boore, 2010).

Except for the BSSA14 model developed for R_{JB} distance, the other ground-motion models used the closest distance to the rupture plane (R_{rup}). As the proposed model in this study is based on the R_{JB} distance metric, we converted R_{rup} to R_{JB} in the ASK14, CB14, CY14, and I14 models using the suggested conversion equations by Scherbaum et al. (2004).

The intensity measures of empirical ground-motion models were obtained for the generic rock site of NEHRP B-C site condition withV_{s30} = 760 m/s. In this study, in order to evaluate the empirical ground motions, a generic style of faulting was used (F_{RV} = 0.5 and F_{NM} = 0 in the ASK14, CB14, and CY14 models, SS = 0.5, RS = 0.5, NS = 0.0, and U = 0.0 in the BSSA14 model, and F = 0.5 in the I14 model are set), and the hanging wall effect was excluded. All models are assessed for the California region, and the default values of certain parameters (assuming no other information was available) suggested by the NGA-West2 model developer are employed. These parameters are Z_{TOR} (the depth to the top of rupture) in the ASK14, CB14, and CY14 models; $Z_{1.0}$, and $Z_{2.5}$ (the depth to the V_S = 1.0 km/s and 2.5 km/s horizon beneath the site, respectively) in the ASK14, BSSA14, and CY14 models.

Proposed GMMs for CENA

Hybrid Empirical Ground-Motion Estimates in CENA

The median hybrid empirical estimates of ground motion for CENA are calculated by applying regional modification factors that properly scale the empirical ground motions in WNA. The model is obtained for the same sets of magnitude (**M**5.0 to **M**8.0 in 0.5 magnitude increments), distances ($2.0 \leq R_{JB} \leq 1000$ km in 33 R_{JB} distances of 2, 5, 10, 15, 20, 30, 40, 50, 60, 70, 80, 90, 100, 110, 120, 140, 150, 160, 180, 200, 250, 300, 350, 400, 450, 500, 550, 600, 650, 700, 800, 900, and 1000 km) and the ground-motion parameters used to obtain empirical GMMs in the host region and to generate synthetics for both the target and host regions.

The regional modification factors are calculated based on the ratios of intensity measures of CENA to WNA. Synthetics are generated and are used to derive the intensity measures in both the target and host regions. In each region, median intensity measures at a particular magnitude, distance, and spectral period are calculated considering all shaking scenarios and all stations distributed in different azimuths. The median intensity measures in CENA are obtained by applying equal weight (1/2) to results from two alternative models as defined in this region.

There are some restrictions and issues which need to be considered in developing the hybrid empirical ground-motion estimates. One refers to the range of validity of empirical ground motions used. ASK14, CB14, and CY14 relations were developed for rupture distance (R_{rup}) up to 300 km, while I14 and BSSA14 are valid for R_{rup} < 150 km and R_{JB} < 400 km. All models are applicable in the magnitude range of **M**3.5–8.5 (except for I14 in which **M** ≥ 5 is considered) for the strike slip faulting mechanism. The V_{S30} is considered in the ranges of 180–1000, 150–1500, 250–1500, 180–1500 m/s, and above 450 m/s in ASK14, BSSA14, CB14, CY14, and I14, respectively, by their model developers. It can be inferred that these empirical ground motions are not valid for distances beyond 300–400 km, so it is inappropriate to implement them beyond that distance range. Another issue arises from the difference of the attenuation rates between the CENA and WNA regions used in the synthetic generations (Table 3).

Considering the abovementioned issues, the hybrid empirical method for CENA is limited to be used in distances up to about 70 km in which reliable hybrid empirical estimates are developed. In order to avoid this constraint and extend our GMM up to 1000 km, the procedure proposed by Campbell (2003) and used by Campbell (2011) and Pezeshk et al. (2011) was followed in this study. The procedure supplements hybrid empirical estimates beyond 70 km by intensity measures of generated synthetics. In this regard, for a given magnitude, the intensity measures of synthetics beyond 70 km are scaled by a factor that fits the hybrid empirical estimate to the median of the synthetics' intensity measure at R_{JB} = 70 km in CENA.

The completed set of hybrid empirical ground-motion estimates are then used to develop GMM in CENA for the distances of 2–1000 km and the magnitudes of 5–8. It includes intensity measures of PGA, PGV, and 5%-damped PSAs at spectral periods of 0.01–10s, which were computed using RotD50 parameters for the generic hard rock site condition with V_{s30} = 3000 m/s. We did not include PGD equations since none of the empirical NGA-West2 GMMs implemented in this study provided such equations in their model. In addition, Boore et al. (2014) observed that low-cut filtering have significant influence on the PGD parameter.

The Functional Form

In this study, our effort was to keep the functional form as similar as that presented in Pezeshk et al. (2011). However, there are two changes to the functional form as compared to the median function of Pezeshk et al. (2011): (1) we used R_{JB} distance instead of rupture distance (R_{rup}) and (2) the range of distance in which the rate of attenuation is decayed has been changed from 70–140 km to 60–120 km based on the recent observation of the recorded data by Boore and Thompson (2015) which is also consistent with our HEM ground-motion estimates. The equation (2) represents our functional form used in this study to predict the median ground motion for CENA:

$$
\begin{aligned}
&\log(\overline{\mathrm{Y}}) = c_1 + c_2\mathbf{M} + c_3\mathbf{M}^2 + (c_4 + c_5\mathbf{M}) \times \min\left\{\log(R), \log(60)\right\} \\
&+(c_6 + c_7\mathbf{M}) \times \max\left[\min\left\{\log(R/60), \log(120/60\right\}, 0\right] \\
&+(c_8 + c_9\mathbf{M}) \times \max\left\{\log(R/120), 0\right\} + c_{10}R
\end{aligned} \tag{2}
$$

and

$$
R = \sqrt{R_{JB}^2 + c_{11}^2} \tag{3}
$$

where $\overline{Y}$ represents the median value of ground-motion intensity measure in CGS units (i.e., PSA (g), PGA (g), or PGV (cm/s)), M is the moment magnitude, R_{JB} (km) is the closest horizontal distance to the vertical projection of the rupture plane, and c_1 to c_{11} are the coefficients of the functional form that fits the hybrid empirical estimates of ground motion in CENA. The coefficients are derived from a nonlinear least-squares regression and are tabulated in Table 7. PSA (g) signifies the pseudo-spectral accelerations for 5% damping and for spectral periods of 0.01–10.0s. The resulting ground-motion model is valid for $5.0 \leq \mathbf{M} \leq 8.0$, 5.0, $2.0 \leq R_{JB} \leq 1000$ km, and is developed for the generic hard rock site with $V_{s30} = 3000$ m/s.

Aleatory and Epistemic Uncertainty Model

Following the standard practice in the U.S., the aleatory variability and epistemic uncertainty in this study are presented in the natural log unit (although the median GMM is proposed in the decimal logs). Therefore, to consider the uncertainty model which will be discussed in this section along with the median GMM shown in equation (2), the adjustment factor between the natural log and base 10 logarithm should be applied.

Aleatory Uncertainty

The aleatory uncertainty characterizes the inherent randomness in the predicted model which is the result of unknown characteristics of the model (Campbell, 2007). In this study, the model for the mean aleatory uncertainty is derived based on the weighted geometric mean of the standard deviations from 5 NGA-West2 GMMs (2/9 to each of the ASK14, BSSA14, CB14, and CY14, and 1/9 to the I14 relations). It is assumed that the median aleatory standard deviation in CENA is equal to the average standard deviation of NGA GMMs for WNA (Campbell, 2003; 2007; Pezeshk et al., 2011):

$$\sigma_{\ln}(\bar{\mathrm{Y}}) = \begin{cases} c_{12}\mathbf{M} + c_{13} & \mathbf{M} \leq 6.5 \\ \psi\mathbf{M} + c_{14} & \mathbf{M} > 6.5 \end{cases} \qquad (4)$$

where ψ = –6.898*E*–03 for PGA (g) and PSAs (g) in the period range of 0.01–10s, and ψ = –3.054*E*–05 for PGV(cm/s).

Coefficients used in equation (4) are provided in Table 8. It should be noted that effects of inter-event and intra-event residuals have been taken into account in the individual uncertainty equations of NGA models. The general form of the standard deviations for CY14 and I14 are magnitude and period dependent. The CB14 model included the site condition (V_{s30}) in addition to magnitude and period in its uncertainty equation. The standard deviation for the BSSA14 and ASK14 models vary with respect to the spectral period, V_{s30}, and magnitude as well as distance. In order to provide a distance-independent equation for the uncertainty, we neglected the small variations of standard deviations over the distance range at any particular magnitude and period, using the mean values (over all distances). In this study, the standard deviations for NGA-West2 GMMs are generated for the generic rock site condition with V_{s30} = 760 m/s (NEHRP B/C site condition). In addition, we neglected the soil nonlinearity effects for the generic rock site in WNA (as it is observed that this effect is insignificant—except for soft soils under strong shaking—on the variation of standard deviations). Based on the abovementioned assumptions, equation (4) is developed which varies with the magnitude and the spectral period. It represents the mean aleatory standard deviation used in this model. Following Pezeshk et al. (2011), the standard deviation of the regression performed to fit the model to the ground-motion estimates ($\sigma_{\mathrm{Re}\,g}$) is also added to the aleatory standard deviation from equation (4). The total aleatory standard deviation ($\sigma^{T}_{\ln(\bar{\mathrm{Y}})}$) is given as:

$$\sigma^{T}_{\ln(\bar{Y})} = \sqrt{\sigma^{2}_{\ln(\bar{Y})} + \sigma^{2}_{\mathrm{Reg}}} \tag{5}$$

The regression standard deviation (σ_{Reg}) in the natural log unit is given in Table 8.

Epistemic Uncertainty

Epistemic uncertainty is a systematic uncertainty which is due to lack of knowledge. Campbell (2003) provided a comprehensive mathematical framework for epistemic uncertainty evaluation. There are two main sources of epistemic uncertainty in the hybrid empirical method: (1) epistemic uncertainty associated with applying different empirical GMMs for the host region (i.e., NGA-West2 GMMs), and (2) epistemic uncertainty originating from using different parameters in the synthetic simulation framework in both the host and target regions.

Campbell (2003) and Tavakoli and Pezeshk (2005) considered the epistemic uncertainty in empirical GMMs in the host region (WNA) through applying different empirical ground-motion models. They also included the uncertainty associated with the seismological parameters used in the synthetic simulations in just the target region (ENA). Campbell (2007) and Atkinson (2008) did not formally evaluate the epistemic uncertainty in their HEM models. Pezeshk et al. (2011) did not evaluate the epistemic uncertainty in their model; however, they incorporated multiple empirical ground-motion models in the host region.

Al Atik and Youngs (2014) presented a distance-independent model of additional epistemic uncertainty to the median prediction of 5 NGA-West2 GMMs by assigning the equal weight to each model in a logic tree framework. Their uncertainty model includes the within-model uncertainty due to data limitations. This uncertainty is derived based on assessment of distance, magnitude, spectral period and faulting mechanism of the NGA-West2 models. For the strike slip faulting mechanism with magnitude less than 7.0 and for spectral periods less than 1.0s, a constant value is assigned. This uncertainty is increased for longer periods and larger magnitude. In the following equations, $\sigma_{\mu \ln(psa)-eps1}$ signifies the epistemic uncertainty associated with using different empirical ground motions in the host region for the strike slip faulting mechanism, and represents the minimum additional epistemic uncertainty required to be implemented into the median ground-motion estimation from these models:

For spectral period less than 1.0 second (T < 1.0s):

$$\sigma_{\mu \ln(psa)-eps1} = \begin{cases} 0.072 & \mathbf{M} < 7 \\ 0.0665(\mathbf{M}-7) + 0.072 & \mathbf{M} \geq 7 \end{cases} \tag{6}$$

For spectral period greater or equal to 1.0 second (T ≥ 1.0s):

$$\sigma_{\mu \ln(psa)-eps1} = \begin{cases} 0.072 + 0.0217\ln(T) & \mathbf{M} < 7 \\ 0.0665(\mathbf{M}-7) + 0.072 + 0.0217\ln(T) & \mathbf{M} \geq 7 \end{cases} \tag{7}$$

where T is the spectral period and $\mathbf{M}$ is the moment magnitude.

The epistemic uncertainty for an individual GMM is infrequently employed (except for the high-risk facility analyses), particularly for a region with available multiple ground-motion models and it requires extensive computations (Campbell 2003; 2007).

Although we have not performed a comprehensive evaluation of the epistemic uncertainty in order to capture and include all the parametric and modeling variations in this study, the uncertainty associated with some parameters used in synthetic simulations (for both target and host regions) is provided. This parametric uncertainty represents the overall variation of the most important seismological parameters used in both stochastic HF and deterministic LF simulations (such as slip velocity distribution, hypocenter location, station location, etc.). The period-dependent parametric uncertainty (σ_{Par}) is given in Table 8.

Equation (8) represents the epistemic uncertainty captured in this study associated with applying empirical ground motions suggested by Al Atik and Youngs (2014) along with the parametric variability in synthetic simulations.

$$\eta^{Sub}_{\ln(\bar{Y})} = \sqrt{\sigma_{\mu\ln(psa)-eps1}{}^2 + \sigma_{Par}{}^2} \tag{8}$$

The total combined uncertainty ($\sigma^{Combined}_{\ln(\bar{Y})}$) that represents both the aleatory variability and epistemic uncertainty is calculated by using the square root of the sum of the squares (SRSS) of equation (5) and equation (8) as:

$$\sigma^{Combined}_{\ln(\bar{Y})} = \sqrt{\sigma^{T}_{\ln(\bar{Y})}{}^2 + \eta^{Sub}_{\ln(\bar{Y})}{}^2} \tag{9}$$

Please note that all equations (4) to (9) are presented in the natural log unit.

Results and Model Evaluation

In this section, the comparison and validation of the product of this study with the previous proposed GMMs as well as the recorded earthquakes in CENA are accomplished.

Figure 2 shows examples of comparison for the 5%-damped response spectral accelerations derived from the hybrid broadband simulations with 5 NGA-West2 GMMs as well as their weighted geometric mean. The response spectra are presented for two magnitudes of **M**6 and 7 at the distance of R_{JB} = 10 km. The WNA spectral accelerations are calculated from the generated broadband synthetics using the parameters discussed earlier. A comparison shows a good agreement between the weighted geometric mean of empirical NGA models and the WNA simulations. In Figure 3, the residuals of the PSAs broadband simulations in WNA and geometric mean of NGA-West2 GMMs with respect to the distance from 2–1000 km for two spectral periods of 0.2s (high frequency) and 4.0s (long period) are shown. The residuals represent a good agreement between the simulations and the empirical ground-motion models in a broad frequency range throughout the distance range.

Comparison with Previous Models

Figure 4 represents the comparison of the GMM developed in this study (hereafter SP15) with three ground-motion models available in CENA: Pezeshk et al. (2011), Atkinson and Boore (2006; 2011), and Pezeshk et al. (2015) [hereafter referred as to PZT11, AB06', and PZCT15, respectively]. The GMM comparisons are given for **M**5 and 7 and for intensity measures of PGA and spectral periods of 0.2, 1.0, and 5.0s in Figure 4. The distance conversion relations for the generic fault style by Scherbaum et al. (2004) is implemented for AB06', PZT11, and PZCT15 in order to compare with the results in this study.

At very close distances for PGA and higher frequency spectral accelerations (e.g., at the spectral period of 0.2s) the magnitude saturation effects are observed in the HEM results of this study. In addition, we perceived over-saturation effects in the results from the broadband synthetics simulations, which is compatible with simulation results from other investigators and observations from the recorded data (Frankel, 2015; Shahjouei and Pezeshk, 2015a). As discussed earlier, the stochastic finite-fault simulations of AB06' and the stochastic point-source model of PZT11 for ENA are based on using the stress parameters of 140 and 250 bars, respectively. The difference in the stress parameter is consistent with the differences between some of the internal assumptions made in SMSIM and EXSIM packages. The PZCT15 model used stress parameter of 400 bars in ENA simulations. The results in this study are derived from the equally weighted simulations in which the stress parameter of 400 and 600 bars in the HF part of synthetics are used. At higher frequencies and close distances, our model provides higher spectral amplitudes than PZT11 and AB06'; however, the results are closer to PZCT15. This could originate from differences between applying stress parameters in different models. At longer periods and close distances, our model predicts lower spectral amplitudes than PZT11 and PZCT15, and the predicted values are closer to AB06'. This could be originated from the application of different earthquake simulations methodologies (i.e., the point-source model for PZT11 and PZCT15, the stochastic finite-fault model for AB06', and HBB for this study) used in the GMM development. The finite-fault models are expected to show a better representation of rupture effects at closer distances.

The response spectral accelerations from the proposed model are compared with those from the AB06', PZT11, and PZCT15 ground-motion models in Figure 5. The spectra are shown for earthquake magnitudes of **M**5, 6, 7, and 8 at a distance of R_{JB} = 20 km for spectral periods up to 10s. At close distances to the fault for the small-to-moderate magnitude earthquakes our model predicted values close to the AB06' but suggested higher values for higher magnitudes. Compared with the PZCT15, our model gives lower amplitudes at longer periods. The difference could originate from the effect of applying the finite-fault approach and using the broadband synthetics in this study (in comparison with the stochastic simulation), particularly at closer distances. The spectral amplitudes in the intermediate period range are affected from both parts of HF and LF synthetics.

Comparison with Recorded Ground Motions

The new model is compared with the NGA-East database (Goulet et al., 2014). In the comparison, the data from the Gulf Coast region and potentially induced events (PIEs) are excluded. In addition, we used the data recorded at stations with $V_{s30} \geq 180$ m/s. Figure 6 shows comparisons of the results of this study with the small-to-moderate magnitude recorded earthquake data available in the NGA-East database. The spectral accelerations in this figure are plotted for the spectral periods of 0.2, 1.0 and 4.0s in different magnitude bins of **M**4.5, 5, and 6. In order to make the appropriate assessment, intensity measures of the NGA-East database are adjusted to the V_{s30} = 3 km/s. This scaling is performed by using the ratios of amplification factors that scale the calculated intensity measures at stations with local shear wave velocities to the reference rock site condition used in this study (i.e., V_{s30} = 3 km/s) similar to the procedure incorporated in PZCT15 GMM development. Comparisons show an overall good agreement between the proposed model and small-to-moderated magnitude recorded data in the NGA-East database.

The magnitude-distance distribution of implemented CENA ground-motion recordings for the comparison and residual analyses is shown in Figure 7. In the comparison, earthquakes with magnitudes **M** ≥ 4 recorded at stations with distances less than 1000 km is considered. Figure 8 depicts the CENA recording stations and earthquakes used for the comparison and residual analyses of this study. As discussed earlier, all potentially induced earthquakes (PIEs) and all stations located within the Gulf Coast region are excluded.

Figures 9 through 11 show examples of the residual analysis performed in this study. The residuals represent the differences between predicted (simulated) and earthquake recorded data in the NGA-East database. Figure 9 shows the distribution of site-adjusted residuals with respect to the distance for spectral accelerations at periods of 0.2, 1.0, and 4s. The mean and 95% confidence limits of the mean binned residuals at 5 distance bins are superimposed in this plot. The distribution of residuals with respect to the magnitude at the same spectral periods is given in Figure 10. In Figure 11 the residuals are decomposed in classified terms of the inter-event (between-event) and intra-event (within-event) residuals for the same periods of 0.2, 1.0, and 4s using the variance-component technique of Chen and Tsai (2002). This classification demonstrates the effects of very small magnitude earthquakes included in the catalog as the total residuals are dependent on the numbers of stations and events in the database. Additionally, the effects of local site condition on residuals are illustrated in this figure. The corrected residuals are obtained after applying scaling factors to represent all intensity measures with the reference rock site condition. The detailed information of the procedure is given in Pezeshk et al. (2015). Residual plots show no discernible trend in residuals obtained from the predicted model and the NGA-East database.

Discussions and Conclusions

A hybrid empirical ground-motion model is proposed for CENA as part of the NGA-East research project. The proposed GMM represents an alternative hybrid empirical model in which a physics-based simulation technique is employed to develop regional adjustment factors compared to previous HEM models that have been developed using stochastic simulation (Campbell, 2003; 2007; Pezeshk et al., 2011). To implement in HEM, earthquake broadband synthetics are generated using the hybrid broadband simulation technique that employs a finite-fault method for both host (WNA) and target (CENA) regions. The HF synthetics are produced using a stochastic finite-fault method, and the LF traces are constructed using kinematic source models and deterministic wave propagation. Two sets of stochastic parameters for CENA are equally weighted and used to consider the variability in parameters. A detailed description of the synthetic generation approach and the parameters used are discussed in the ground-motion simulation part and are also available in Shahjouei and Pezeshk (2015a). For synthetic simulations we used the updated seismological and geological parameters suggested in the literature.

Five recent empirical ground-motion models of ASK14, BSSA14, CB14, CY14, and I14, developed as part of the NGA-West2 project, were incorporated in this study. These empirical models are weighted following the procedure adopted by the 2014 USGS NSHMs (Petersen et al., 2014).

The new ground-motion model is developed for R_{JB} distances up to 1000 km, for the moment magnitude range of **M**5–8, and for the suggested generic hard rock site condition with V_{s30} = 3000 m/s (Hashash et al., 2014) for CENA. Applying the proper site amplification factors available in the literature such as the inverse of the method used to adjust the NGA-East database recordings to the reference hard rock site conditions (Pezeshk et al., 2015), a ground-motion model could be estimated for other site conditions with different V_{s30} values.

The new GMM is compared with the ground-motion models of Pezeshk et al. (2011), Atkinson and Boore (2006; 2011), and Pezeshk et al. (2015). The inter-event and intra-event residuals that represent the differences between the predicted and observed ground-motion intensity measures display no discernible trend. The residual analyses are performed on the small-to-moderate earthquakes in CENA available in the NGA-East dataset with respect to the magnitude and distance.

The new sets of coefficients are provided to be used in the functional form of the GMM. The uncertainties associated with the new model are discussed and provided. The aleatory variability and epistemic uncertainty incorporated the uncertainties in NGA-West2 GMMs and the regression analysis used to derive the GMM coefficients. The minimum additional epistemic uncertainty suggested to be used along with the median of NGA-West2 GMMs (Al Atik and Youngs, 2014) as well as the variation of some parametric modeling are provided in this study. The authors suggest to use the total combined uncertainty as shown in equation (9) where the proposed GMM is employed as stand-alone, and apply the total aleatory standard deviation as represented in equation (5) in conjunction with alternative GMMs in order to avoid double counting of uncertainty. The proposed ground-motion relation, as an alternative GMM, together with the other available models can be implemented in order to better characterize the ground-motion estimations and to effectively signify the epistemic uncertainty in the CENA.

Data and Resources

The COMPSYN sxv3.11 software package provided by its author (Dr. Paul Spudich) is used for long period simulations. We have used and modified the rupture model generator package by Dr. Martin Mai (some codes are available at www.ces.kaust.edu.sa/Pages/Software.aspx, last accessed August 2013). The SMSIM program and TSPP Fortran software package available at www.daveboore.com (last accessed May 2013) have been incorporated in this study. The NGA-East database for comparison is obtained at https://www.dropbox.com/sh/3sbwbfymiltztuj/AAAyene-Bj460E0pE39h-9FEa?dl=0 (last accessed September 12, 2014).

Acknowledgments

The authors would like to acknowledge Paul Spudich and Martin Mai (and his team Kiran K. Thingbaijam and Hugo C. Jimenez) for providing us with their software packages and their continuous support and suggestions which helped us in earthquake simulations. We have benefitted from discussions and interactions with, and comments received from, Kenneth Campbell, Christine Goulet, and the NGA-East TI team. We also would like to thank Cezar I. Trifu and one anonymous reviewer for their constructive comments and suggestions which helped us to improve the manuscript.

References

Abrahamson, N. A., and W. J. Silva (2001). Empirical attenuation relations for central and eastern U.S. hard and soft rock and deep soil site conditions (abstract), *Seism. Res. Lett.* **72**, 282.

Abrahamson, N. A., W. J. Silva, and R. Kamai (2014). Summary of the ASK14 ground motion relation for active crustal regions, *Earthq. Spectra* **30**(3), 1025–1055.

Al Atik, L., and R. R. Youngs (2014). Epistemic uncertainty for NGA-West2 models, *Earthq. Spectra* **30**(3), 1301–1318.

Al Atik, L., A. Kottke, N. A. Abrahamson, and J. Hollenback (2014). Kappa (k) scaling of ground-motion prediction equations using an inverse random vibration theory approach, *Bull. Seismol. Soc. Am*. **104**, 336–346.

Anderson, J. G. (2015). The composite source model for broadband simulations of strong ground motions, *Res. Lett*. **86**(1), 68–74.

Andrews, D. J. (1980). A stochastic fault model: 1. Static case, *J. Geophys. Res.*, **85**, 3867–3877.

Atkinson, G. M. (2001). An alternative to stochastic ground-motion relations for use in seismic hazard analysis in eastern North America, *Seism. Res. Lett.* **72**, 299–306.

Atkinson, G. M. (2004). Empirical attenuation of ground motion spectral amplitudes in southeastern Canada and the northeastern United States, *Bull. Seismol. Soc. Am*. **94**, 1079–1095.

Atkinson, G. M. (2008). Ground-motion prediction equations for eastern North America from a referenced empirical approach: implications for epistemic uncertainty, *Bull. Seismol. Soc. Am*. **98**, 1304–1318.

Atkinson, G. M., and W. J. Silva (1997). An empirical study of earthquake source spectra for California earthquakes, *Bull. Seismol. Soc. Am*. **87**, 97–113.

Atkinson, G. M., and D. M. Boore (1998). Evaluation of models for earthquake source spectra in eastern North America, *Bull. Seismol. Soc. Am*. **88**, 917–934.

Atkinson, G. M., and W. J. Silva (2000). Stochastic modeling of California ground motions, *Bull. Seismol. Soc. Am*. **90**, 255–274.

Atkinson, G. M., and D. M. Boore (2006). Earthquake ground-motion prediction equations for eastern North America, *Bull. Seismol. Soc. Am*. **96**(6), 2181–2205.

Atkinson, G. M., K. Assatourians, D. M. Boore, K. Campbell, and D. Motazedian (2009). A guide to differences between stochastic point-source and stochastic finite-fault simulations, *Bull. Seismol. Soc. Am*. **99**(6), 3192–3201.

Atkinson, G. M., and D. M. Boore (2011). Modification to existing ground motion prediction equations in light of new data, *Bull. Seismol. Soc. Am*. **101**(3), 1121–1135.

Atkinson, G. M., and D. M. Boore (2014). The attenuation of Fourier amplitudes for rock sites in eastern North America, *Bull. Seismol. Soc. Am*. **104**(1), 513–528.

Atkinson, G. M., and K. Assatourians (2015). Implementation and validation of EXSIM (a stochastic finite-fault ground-motion simulation algorithm) on the SCEC broadband platform, *Seis. Res. Lett*. **86**(1), 48–60.

Beresnev, I. A., and G. M. Atkinson (2002). Source parameters of earthquakes in eastern and western North America based on finite–fault modeling, *Bull. Seismol. Soc. Am*. **92**, 695–710.

Boore, D. M. (1983). Stochastic simulation of high-frequency ground motions based on seismological models of the radiated spectra, *Bull. Seismol. Soc. Am*. **73**, 1865–1894.

Boore, D. M. (2003). Simulation of ground motion using the stochastic method, *Pure Appl. Geophys.* **160**: 635–676.

Boore, D. M. (2009). Comparing stochastic point-source and finite-source ground-motion simulations: SMSIM and EXSIM, *Bull. Seismol. Soc. Am*. **99**(6), 3202–3216.

Boore, D. M. (2010). Orientation-independent, non-geometric-mean measures of seismic intensity from two horizontal components of motion, *Bull. Seismol. Soc. Am*. **100**, 1830–1835.

Boore, D. M. (2012). SMSIM; FORTRAN programs for simulating ground motions from earthquakes: Update version of 11/02/2012; www.daveboore.com (last accessed August 2013).

Boore, D. M., and W. B. Joyner (1997). Site amplification for generic rock sites, *Bull. Seismol. Soc. Am*. **87**, 327–341.

Boore, D. M., J. Watson-Lamprey, and N. A. Abrahamson (2006). Orientation-independent measures of ground motion, *Bull. Seismol. Soc. Am*. **96**, 1502–1511.

Boore, D. M., K. W. Campbell, and G. M. Atkinson (2010). Determination of stress parameters for eight well-recorded earthquakes in eastern North America, *Bull. Seismol. Soc. Am.* **100**, 1632–1645.

Boore, D. M., and E. M. Thompson (2014). Path duration for use in the stochastic-method simulation of ground motions, *Bull. Seismol. Soc. Am.* **104**, 2541–2552.

Boore, D. M., J. P. Stewart, E. Seyhan, and G. M. Atkinson (2014). NGA-West2 equations for predicting PGA, PGV, and 5% damped PSA for shallow crustal earthquakes, *Earthq. Spectra* **30**(3), 1057–1085.

Boore, D. M., and E. M. Thompson (2015). Revisions to some parameters used in stochastic method simulations of ground motion, *Bull. Seismol. Soc. Am.* **105**, 1029–1041.

Bozorgnia, Y., and K. W. Campbell (2004). Engineering characterization of ground motion, Book Chapter 5, *Earthquake Engineering: From Engineering Seismology to Performance-Based Engineering*, Bozorgnia, Y., and V. V. Bertero (Editors), CRC Press, MA, USA.

Bozorgnia, Y., and 30 other authors (2014). NGA-West2 research project, *Earthq. Spectra* **30**(3), 973–987.

Campbell, K. W. (1981). A ground motion model for the central United States based on near source acceleration data, in Proceedings of the Conference on Earthquakes and Earthquake Engineering—the Eastern United States, Ann Arbor Science Publishers, Ann Arbor, MI, Vol. 1, 213–232.

Campbell, K. W. (2003). Prediction of strong ground motion using the hybrid empirical method and its use in the development of ground-motion (attenuation) relations in eastern North America, *Bull. Seismol. Soc. Am.* **93**, 1012–1033.

Campbell, K. W. (2007). Validation and update of hybrid empirical ground motion (attenuation) relations for the CEUS, report to the U.S. Geological Survey, *National Earthquake Hazards Reduction External Research Program*, Award No. 05HQGR0032.

Campbell, K.W. (2011). Ground motion simulation using the hybrid empirical method: Issues and insights, in *Earthquake Data in Engineering Seismology: Predictive Models, Data Management and Networks,* S. Akkar, P. Gulkan, and T. van Eck (Editors), Geotechnical, Geological and Earthquake Engineering Series, Springer, London, 14: 81–95.

Campbell, K. W. (2014). An evaluation of eastern North America ground-motion models developed using the hybrid empirical method, *Bull. Seismol. Soc. Am.* **104**, 347–359.

Campbell, K. W., and Y. Bozorgnia (2014). NGA-West2 ground motion model for the average horizontal components of PGA, PGV, and 5% damped linear acceleration response spectra, *Earthq. Spectra* **30**(3), 1087–1115.

Chapman, M. C, S. Pezeshk, M. Hosseini, and A. Conn (2014). Regional study of Fourier amplitude drop of *Lg*-wave acceleration in central United States*, Seismol. Res. Lett*., **85**, 513.

Chen, Y. H., and C. P. Tsai (2002). A new method of estimation of the attenuation relationship with variance components, *Bull. Seismol. Soc. Am*., **92**, 1984–1991.

Chiou, B. S., and R. R. Youngs (2014). Update of the Chiou and Youngs NGA model for the average horizontal component of peak ground motion and response spectra, *Earthq. Spectra* **30**(3), 1117–1153.

Crempien, J. G. F., and R. J. Archuleta (2015). USCB method for simulation of broadband ground motion from kinematic earthquake sources, *Res. Lett*. **86**(1), 61–67.

Douglas, J. (2003). Earthquake ground motion estimation using strong-motion records: A review of equations for the estimation of peak ground acceleration and response spectral ordinates, *Earth-Science Reviews*, **61**(1–2), 43–104.

Douglas, J. (2011). Ground motion prediction equations 1964–2010, *PEER Report 2011/102,* Berkeley, CA.

Douglas, S. D., G. C. Beroza, S. M. Day, C. A. Goulet, T. H. Jordan, P. A. Spudich, and J. P. Stewart (2015). Validation of SCEC broadband platform V14.3 simulation methods using pseudo spectral acceleration data, *Seis. Res. Lett.* **86**(1), 39–47.

Frankel, A. (1995). Simulating strong motions of large earthquakes using recordings of small earthquakes: The Loma Prieta mainshock as a test case, *Bull. Seismol. Soc. Am*. **85**, 1144–1160.

Frankel, A. (2009). A constant stress-drop model for producing broadband synthetic seismograms: Comparison with the Next Generation Attenuation relations, *Bull. Seismol. Soc. Am.* **99**, 664–680.

Frankel, A. (2015). Ground-motion prediction equations for eastern North America earthquakes using the hybrid broadband seismograms from finite-fault simulations with constant stress-drop scaling, in Chapter 6 of "NGA-East: Median ground-motion models for the central and eastern North America region," *PEER Report 2015/04,* Berkeley, CA.

Frankel, A., C. Muller, T. Barnhard, D. Perkins, E.V. Leyendecker, N. Dickman, S. Hanson, and M. Hooper (1996). National Seismic-Hazard Maps, *U.S. Geological Survey,* Open-File Report 96-532, 100 pp.

Ghodrati, G., A. Shahjouei, S. Saadat, and M. Ajallooeian (2011). Implementation of genetic algorithm, MLFF neural network, principal component analysis, and wavelet packet transform in generation of compatible seismic ground acceleration time histories. *J. Earthq. Eng.* **15**(1), 50–76.

Goulet, C. A., T. Kishida, T. D. Ancheta, C. H. Cramer, R. B. Darragh, W. J. Silva, Y. M. A. Hashah, J. Harmon, J. P. Stewart, K. E. Wooddell, and R. R. Youngs (2014). PEER NGA-East database, *PEER Report 2014/17*, Berkeley, CA.

Goulet, C. A., N. A. Abrahamson, P. G. Somerville, and K. E. Wooddell (2015). The SCEC broadband platform validation exercise: methodology for code validation in the context of seismic-hazard analysis, *Seis. Res. Lett.* **86**(1), 17–26.

Graves, R. W., and A. Pitarka (2004). Broadband time history simulation using a hybrid approach*, Proc. 13th World Conf. Earthq. Eng*., Vancouver, Canada, paper no. 1098, Aug 1–6.

Graves, R. W., and A. Pitarka (2010). Broadband ground-motion simulation using a hybrid approach*, Bull. Seismol. Soc. Am.* **100**(5A), 2095–2123.

Graves, R., and A. Pitarka (2015). Refinements to the Graves and Pitarka (2010) broadband ground-motion simulation method, *Res. Lett*. **86**(1), 75–80.

Hanks, T. C., and R. K. McGuire (1981). The character of high–frequency strong ground motion, *Bull. Seismol. Soc. Am*. **71**, 2071–2095.

Hanks, T. C., and W. H. Bakun (2002). A bilinear source-scaling model for M–log A observations of continental earthquakes, *Bull. Seismol. Soc. Am*. **92**, 1841–1846.

Hartzell, S. H., M. Guatteri, G. Mariagiovanna, P. M. Mai, P-C. Liu, and M. Fisk (2005). Calculation of broadband time histories of ground motion, Part II: Kinematic and dynamic modeling using theoretical Green's functions and comparison with the 1994 Northridge earthquake, *Bull. Seismol. Soc. Am*. **95**, 614–645.

Hashash, Y. M. A., A. R. Kottke, J. P. Stewart, K. W. Campbell, B. Kim, C. Moss, S. Nikolaou, E. M. Rathje, and W. J. Silva (2014). Reference rock site condition for central and eastern North America, *Bull. Seismol. Soc. Am*. **104**, 684–701.

Herrmann, R. B. (1985). An extension of random vibration theory estimates of strong ground motion to large distances, *Bull. Seismol. Soc. Am*. **75**, 1447–1453.

Idriss, I. M. (2014). An NGA-West2 empirical model for estimating the horizontal spectral values generated by shallow crustal earthquakes, *Earthq. Spectra* **30**(3), 1155–1177.

Kramer S. L. (1996). Geotechnical earthquake engineering, Prentice Hall, Upper Saddle River, NJ, 653 pp.

Liu, P., R. Archuleta, and S. H. Hartzell (2006). Prediction of broadband ground motion time histories: Frequency method with correlation random source parameters, *Bull. Seismol. Soc. Am*. **96**, 2118–2130.

Mai, P. M., and G. C. Beroza (2000). Source scaling properties from finite-fault rupture models, *Bull. Seismol. Soc. Am*. **90**(3), 604–615.

Mai, P. M., and G. C. Beroza (2002). A spatial random field model to characterize complexity in earthquake slip, *J. Geophys. Res*. **107**, no. B11, 2308.

Mai, P. M., P. Spudich, and J. Boatwright (2005). Hypocenter locations in finite-source rupture models, *Bull. Seismol. Soc. Am*. **95**, 965–980.

Mai, P. M., W. Imperatori, and K. B. Olsen (2010). Hybrid broadband ground-motion simulations: Combining long-period deterministic synthetics with high-frequency multiple S-to-S backscattering, *Bull. Seismol. Soc. Am.* **100**(5), 2124–2142.

Malagnini, L., K. Mayeda, R. Uhrhammer, A. Akinci, and R. B. Herrmann (2007). A regional ground-motion excitation/attenuation model for the San Francisco region, *Bull. Seismol. Soc. Am*. **97**, 843–862.

Mena, B., P. M. Mai, K. B. Olsen, M. D. Purvance, and J. N. Brune (2010). Hybrid broadband ground-motion simulation using scattering Green's functions: Application to large-magnitude events, *Bull. Seismol. Soc. Am.* **100**(5A), 2143–2162.

Mooney, W., D. G. Chulick, A. Ferguson, A. Radakovich, K. Kitaura, and S. Detweiler (2012). NGA-East: Crustal Regionalization. NGA-East working meeting: Path and Source Issues, Oct. 16 2012, UC Berkeley.

Motazedian, D., and G. M. Atkinson (2005). Stochastic finite-fault modeling based on a dynamic corner frequency*, Bull. Seismol. Soc. Am*. **95**, 995–1010.

Nuttli, O. W., and R. B. Herrmann (1984). Ground motion of Mississippi Valley earthquakes, *J. Tech. Topics Civil Eng.* **110**, 54–69.

Olsen, K. B. (2012). 3D broadband ground motion estimation for large earthquakes on the New Madrid seismic zone, Central US, *final report to the U.S. Geological Survey*, Award # G10AP00007.

Olsen, K. B., and R. Takedatsu (2015). The SDSU broadband ground-motion generation module BBtoolbox version 1.5, *Res. Lett*. **86**(1), 81–88.

Petersen, M. D., M. P. Moschetti, P. M. Powers, C. S. Mueller, K. M. Haller, A. D. Frankel, Y. Zeng, S. Rezaeian, S. C. Harmsen, O. S. Boyd, N. Field, R. Chen, K. S. Rukstales, N. Luco, R. L. Wheeler, R. A. Williams, and A. H. Olsen (2014). Documentation for the 2014 update of the United States national seismic hazard maps: *U.S. Geological Survey Open-File Report* 2014–1091, 243.

Pezeshk, S., A. Zandieh, and B. Tavakoli (2011). Hybrid empirical ground-motion prediction equations for Eastern North America using NGA models and updated seismological parameters, *Bull. Seismol. Soc. Am*. **101**(4), 1859–1870.

Pezeshk, S., A. Zandieh, K. Campbell, and B. Tavakoli (2015). Ground-motion prediction equations for CENA using the hybrid empirical method in conjunction with NGA-West2 empirical ground-motion models, in Chapter 5 of "NGA-East: Median ground-motion models for the central and eastern North America region," PEER Report # 2015/04.

Power, M., B. Chiou, N. A. Abrahamson, Y. Bozorgnia, T. Shantz, and C. Roblee (2008). An overview of the NGA project, *Earthquake Spectra* **24**, 3–21.

Raoof, M., R. B. Herrmann, and L. Malagnini (1999). Attenuation and excitation of three–component ground motion in southern California, *Bull. Seismol. Soc. Am*. **89**, 888–902.

Ripperger, J., and P. M. Mai (2004). Fast computation of static stress changes on 2D faults from final slip distributions, *Geophys. Res. Lett.* **31**(18), L18610, doi:10.1029/2004GL020594.

Scherbaum, F., J. Schmedes, and F. Cotton (2004). On the conversion of source-to-site distance measures for extended earthquake source models, *Bull. Seismol. Soc. Am.* **94**(3), 1053–1069.

Shahjouei, A., and S. Pezeshk (2015a). Synthetic seismogram simulations using a hybrid broadband ground-motion simulation approach: Application to central and eastern United States, *Bull. Seismol. Soc. Am.* **105**(2), 686–705.

Shahjouei, A., and S. Pezeshk (2015b). Hybrid empirical ground-motion model for central and eastern North America using hybrid broadband simulations and NGA-West2 GMPES, in Chapter 7 of “NGA-East: Median ground-motion models for the central and eastern North America region,” PEER Report # 2015/04.

Siddiqqi, J., and G. M. Atkinson (2002). Ground motion amplification at rock sites across Canada, as determined from the horizontal-to-vertical component ratio, *Bull. Seismol. Soc. Am*. **92**, 877–884.

Silva, W. J., N. Gregor, and R. Darragh (2002). Development of regional hard rock attenuation relations for central and eastern North America, *Pacific Engineering and Analysis Technical Report*, 57 pp.

Somerville, P. (2006). Review of magnitude-area scaling of crustal earthquakes, Report to Working Group on California Earthquake Probabilities, 22 pp. URS Corp., Pasadena, CA.

Somerville, P., K. Irikura, R. Graves, S. Sawada, D. Wald, N. Abrahamson, Y. Iwasaki, N. Smith, and A. Kowada (1999). Characterizing crustal earthquake slip models for the prediction of strong ground motion, *Seism. Res. Lett.* **70**, 59–80.

Somerville, P., N. Collins, N. Abrahamson, R. Graves, and C. Saikia (2001). Ground motion attenuation relations for the central and eastern United States, *Report to U.S. Geological Survey*, NEHRP External Research Program, Award # 99-HQ-GR-0098.

Somerville, P. G., R. W. Graves, N. F. Collins, S. G. Song, S. Ni, and P. Cummins (2009). Source and ground motion models of Australian earthquakes, proceedings of the 2009 Annual Conference of the Australian Earthquake Engineering Society, Newcastle, UK, Dec. 11–13.

Spudich, P., and L. Xu (2003). Software for calculating earthquake ground motions from finite-faults in vertically varying media, in *IASPEI International Handbook of Earthquake and Engineering Seismology*, W. H. K. Lee, H. Kanamori, P. C. Jennings, and C. Kisslinger (Editors), Chapter 85.14, Academic Press, New York, 1633–1634.

Stanislavsky, E., and G. Garven (2002). The minimum depth of fault failure in compressional environments, *Geophys. Res. Lett.* **29**(24), 2155.

Stirling, M. W. (2014). The continued utility of probabilistic seismic-hazard assessment, Book Chapter 13, *Earthquake Hazard, Risk and Disaster,* Shroder, J. F., and M. Wyss (Editors), Academic Press, Waltham, MA, 359–376.

Tavakoli, B., and S. Pezeshk (2005). Empirical-stochastic ground-motion prediction for Eastern North America, *Bull. Seismol. Soc. Am*. **95**(6), 2283–2296.

Tinti, E., E. Fukuyama, A. Piatanesi, and M. Cocco (2005). A kinematic source-time function compatible with earthquake dynamics, *Bull. Seismol. Soc. Am*. **95**, 1211–1223.

Toro, G. R. (2002). Modification of the Toro et al. (1997) attenuation equations for large magnitudes and short distances: Risk Engineering Technical Report, 10 pp.

Toro, G. R., N. A. Abrahamson, and J. F. Schneider (1997). Model of strong ground motions from earthquakes in central and eastern North America: Best estimates and uncertainties*,* *Seis. Res. Lett*. **68**, 41–57.

Wells, D. L., and K. J. Coppersmith (1994). New empirical relationships among magnitude, rupture length, rupture width, and surface displacements, *Bull. Seismol. Soc. Am*. **84**, 974-1002.

Working Group on California Earthquake Probabilities (2003). Earthquake probabilities in the San Francisco Bay region, 2002-2031, *U.S. Geological Survey Open-File Report* 03-214, 235 pp.

Yenier, E., and G. M. Atkinson (2014). Equivalent point-source modeling of moderate to large magnitude earthquakes and associated ground-motion saturation effects, *Bull. Seismol. Soc. Am*. **104**, 1458–1478.

Zandieh, A., S., Pezeshk, and K. W. Campbell (2015). An equivalent point-source stochastic model of small-to-moderate magnitude earthquakes in California from NGA-West2 ground motion prediction equations, *Bull. Seismol. Soc. Am*., in preparation.

Zeng, Y., J. G. Anderson, and G. Yu (1994). A composite source model for computing realistic synthetic strong ground motions, *Geophys. Res. Lett*. **21**, 725-728.

Mailing Address of the Authors

Alireza Shahjouei, Ph.D. Candidate
Shahram Pezeshk, Professor
3815 Central Ave., Department of Civil Engineering
The University of Memphis, Memphis, TN 38152

List of Tables:

List of Figures

Table 1. The rupture geometry used in synthetic simulations.

M	CENA (km)				WNA (km)			
	L	W	Z_{TOR}	Z_{Hypo}	L	W	Z_{TOR}	Z_{hypo}
5.0	2	3	3–5	6.5±1.5	3.0	4	3–4	6.0±1.0
5.5	5	5	3–5	7.5±2.0	4.5	4.5	3–4	6.5±1.0
6.0	8	6	3–5	8.0±1.5	12	7	3–4	8.5±1.0
6.5	18	12	2–4	11.0±1.5	18	12	2–3	12±1.5
7.0	23	12	2–4	11.0±1.5	50	13	2–3	12±1.5
7.5	150	15	2–3	12.0±2.0	150	15	1–2	13.5±2
8.0	150	22	2–3	17.0±2.0	180	25	1–2	18±2

Table 2. Summary of some parameters implemented in long period synthetic simulations.

M	$\log_{10}(M_0)$ (N. m)	f_{cross} (Hz)	CENA		WNA	
			Ave. Slip (m)	Ave. Rise Time (s)	Ave. Slip (m)	Ave. Rise Time (s)
5.0	16.550	3.0	0.18	0.21	0.10	0.12
5.5	17.301	3.0	0.25	0.38	0.25	0.20
6.0	18.041	2.6	0.71	0.67	0.40	0.36
6.5	18.799	2.4	0.90	1.20	0.88	0.64
7.0	19.550	1.6	2.56	2.12	1.65	1.13
7.5	20.300	0.8	2.70	3.75	2.68	2.02
8.0	21.050	0.8	10.3	6.72	7.56	3.58

Table 3. The median parameters used in high-frequency stochastic synthetic simulations for CENA and WNA.

Parameter	CENA-Alternative 1 (1/2)	CENA-Alternative 2 (1/2)	WNA
Source spectrum model	Single corner frequency ω^{-2}	Single corner frequency ω^{-2}	Single corner frequency ω^{-2}
Stress parameter, $\Delta\sigma$ (bars)	600	400	135
Shear-wave velocity at source depth, β_s (km/s)	3.7	3.7	3.5
Density at source depth, ρ_s (gm/cc)	2.8	2.8	2.8
Geometric spreading, *Z (R)*	$\begin{cases} R^{-1.3} & R < 50km \\ R^{-0.5} & R \geq 50km \end{cases}$	$\begin{cases} R^{-1.3} & R < 60km \\ R^{0} & 60 \leq R < 120km \\ R^{-0.5} & R \geq 120km \end{cases}$	$\begin{cases} R^{-1.03} & R < 45km \\ R^{-0.96} & 45 \leq R < 125km \\ R^{-0.5} & R \geq 125km \end{cases}$
Quality factor, Q	$525 f^{0.45}$	$440 f^{0.47}$	$202 f^{0.54}$
Source duration, T_s (s)	$1/f_a$	$1/f_a$	$1/f_a$
Path duration, T_p (s)	$\begin{cases} 0 & R \leq 10km \\ +0.16R & 10 < R \leq 70km \\ -0.03R & 70 < R \leq 130km \\ +0.04R & R > 130km \end{cases}$	Boore and Thompson (2015) Table 2	Boore and Thompson (2015) Table 1
Site amplification, *A(f)*	Boore and Thompson (2015) Table 4	Boore and Thompson (2015) Table 4	Atkinson and Boore (2006) Table 4
Kappa, k_0 (s)	0.005	0.006	0.035

Table 4. The number of stations where the synthetic seismograms are generated. The statio distributed in the distance and azimuth.

M	R≤200 km		R>200 km	Total	
	CENA	WNA	Both Regions	CENA	WNA
5.0	346	342	140	486	482
5.5	384	384	140	524	384
6.0	380	363	140	520	363
6.5	438	438	140	578	438
7.0	404	355	140	544	355
7.5	459	459	140	599	459
8.0	520	459	140	660	459

Table 5. The crustal structure model used in simulations for WNA (Source: Frankel, 2009) modifications for V_{S30} compatible with referee rock condition in the region.

Z (km)	V_p *(km/s)*	V_s *(km/s)*	ρ *(g/cm³)*
0.0	1.4	0.76	2.1
0.1	2.6	1.60	2.1
0.2	3.3	1.90	2.1
0.3	4.0	2.00	2.4
1.3	5.5	3.20	2.7
3.8	6.3	3.60	2.8
18.0	6.8	3.90	2.9
30.0	7.8	4.50	3.3

Table 6. The mid-continent crustal structure model used in simulations for CENA (Source: Mooney et al., 2012; 2013) with modifications for V_{S30} compatible with referee rock condition in the region.

Z (km)	V_p *(km/s)*	V_s *(km/s)*	ρ *(g/cm^3)*
0.0	5.2	3.0	2.52
1.0	6.1	3.52	2.74
10.0	6.5	3.75	2.83
20.0	6.7	3.87	2.88
40.0	8.1	4.68	3.33

Table 7. Regression coefficients for the proposed hybrid empirical model used to calculate the median ground-motion model (in base 10 log unit).

T (s)	c_1	c_2	c_3	c_4	c_5	c_6	c_7	c_8	c_9	c_{10}	c_{11}
PGA	-0.3002	5.066E-01	-4.526E-02	-3.2240	2.998E-01	-1.283E+00	1.045E-01	-3.0856	2.778E-01	-7.711E-04	3.810E+00
PGV	-2.3891	1.259E+00	-7.901E-02	-2.9386	3.034E-01	-9.290E-03	-4.605E-02	-2.7548	3.467E-01	-7.623E-04	-4.598E+00
0.010	-0.3472	4.838E-01	-4.093E-02	-3.0832	2.712E-01	-9.676E-01	4.983E-02	-2.9695	2.693E-01	-6.695E-04	-4.434E+00
0.020	0.8320	1.934E-01	-2.060E-02	-3.1134	2.786E-01	-1.133E+00	5.994E-02	-3.5023	2.901E-01	-5.857E-04	-4.412E+00
0.030	1.1850	1.064E-01	-1.423E-02	-3.1029	2.792E-01	-1.078E+00	5.239E-02	-3.5722	2.865E-01	-6.220E-04	-4.353E+00
0.040	1.2460	8.986E-02	-1.268E-02	-3.0785	2.773E-01	-9.743E-01	4.160E-02	-3.5083	2.769E-01	-6.818E-04	-4.303E+00
0.050	1.1793	1.037E-01	-1.321E-02	-3.0488	2.744E-01	-8.635E-01	3.077E-02	-3.3986	2.659E-01	-7.439E-04	-4.266E+00
0.075	0.8045	1.866E-01	-1.788E-02	-2.9697	2.660E-01	-6.122E-01	7.491E-03	-3.0852	2.391E-01	-8.801E-04	-4.214E+00
0.100	0.3500	2.871E-01	-2.381E-02	-2.8940	2.576E-01	-4.123E-01	-1.012E-02	-2.7947	2.163E-01	-9.848E-04	4.201E+00
0.150	-0.5264	4.782E-01	-3.519E-02	-2.7610	2.426E-01	-1.319E-01	-3.338E-02	-2.3312	1.818E-01	-1.125E-03	4.239E+00
0.200	-1.2884	6.413E-01	-4.486E-02	-2.6504	2.301E-01	4.637E-02	-4.690E-02	-1.9927	1.576E-01	-1.209E-03	4.325E+00
0.250	-1.9422	7.789E-01	-5.295E-02	-2.5573	2.196E-01	1.631E-01	-5.478E-02	-1.7399	1.398E-01	-1.258E-03	4.438E+00
0.300	-2.5071	8.961E-01	-5.976E-02	-2.4780	2.107E-01	2.407E-01	-5.919E-02	-1.5470	1.265E-01	-1.286E-03	4.571E+00
0.400	-3.4360	1.085E+00	-7.059E-02	-2.3495	1.961E-01	3.244E-01	-6.197E-02	-1.2793	1.085E-01	-1.304E-03	-4.872E+00
0.500	-4.1699	1.231E+00	-7.878E-02	-2.2510	1.849E-01	3.544E-01	-6.046E-02	-1.1111	9.757E-02	-1.294E-03	-5.211E+00
0.750	-5.4797	1.482E+00	-9.245E-02	-2.0865	1.659E-01	3.284E-01	-4.979E-02	-0.9131	8.570E-02	-1.219E-03	-6.154E+00
1.000	-6.3464	1.641E+00	-1.006E-01	-1.9931	1.546E-01	2.530E-01	-3.709E-02	-0.8641	8.405E-02	-1.123E-03	-7.174E+00
1.500	-7.4087	1.823E+00	-1.093E-01	-1.9162	1.438E-01	9.019E-02	-1.551E-02	-0.9200	9.103E-02	-9.407E-04	-9.253E+00
2.000	-8.0057	1.916E+00	-1.130E-01	-1.9173	1.418E-01	-3.828E-02	-1.252E-03	-1.0327	1.016E-01	-7.926E-04	-1.122E+01
3.000	-8.5793	1.985E+00	-1.146E-01	-2.0184	1.499E-01	-1.744E-01	9.393E-03	-1.2453	1.214E-01	-5.919E-04	1.438E+01
4.000	-8.8246	1.990E+00	-1.131E-01	-2.1475	1.635E-01	-1.844E-01	3.919E-03	-1.3849	1.357E-01	-4.855E-04	1.619E+01
5.000	-8.9855	1.975E+00	-1.105E-01	-2.2496	1.764E-01	-1.043E-01	-1.187E-02	-1.4511	1.446E-01	-4.439E-04	1.671E+01
7.500	-9.3927	1.925E+00	-1.032E-01	-2.3572	1.973E-01	3.465E-01	-7.832E-02	-1.3728	1.490E-01	-5.176E-04	1.458E+01
10.000	-9.7350	1.879E+00	-9.666E-02	-2.4139	2.117E-01	1.010E+00	-1.678E-01	-1.0631	1.370E-01	-7.420E-04	1.123E+01

Table 8. The parameters used to calculate the aleatory variability and parametric modeling uncertainty developed in this study (in natural log unit).

T (s)	c_{12}	c_{13}	c_{14}	σ_{Reg}	σ_{Par}
PGA	-5.54E-02	9.78E-01	6.63E-01	1.00E-01	2.88E-01
PGV	-4.10E-02	8.76E-01	6.11E-01	1.94E-01	3.73E-01
0.010	-5.60E-02	9.82E-01	6.64E-01	1.32E-01	2.81E-01
0.020	-5.59E-02	9.83E-01	6.65E-01	9.28E-02	2.81E-01
0.030	-5.77E-02	1.00E+00	6.76E-01	8.33E-02	2.77E-01
0.040	-5.77E-02	1.01E+00	6.88E-01	7.98E-02	2.79E-01
0.050	-5.78E-02	1.03E+00	7.01E-01	7.76E-02	2.72E-01
0.075	-5.61E-02	1.03E+00	7.21E-01	7.38E-02	2.52E-01
0.100	-5.65E-02	1.05E+00	7.32E-01	7.17E-02	2.65E-01
0.150	-5.59E-02	1.04E+00	7.24E-01	7.16E-02	2.76E-01
0.200	-5.60E-02	1.03E+00	7.15E-01	7.43E-02	2.58E-01
0.250	-5.37E-02	1.02E+00	7.12E-01	7.79E-02	2.68E-01
0.300	-5.11E-02	1.01E+00	7.18E-01	8.15E-02	2.84E-01
0.400	-4.70E-02	9.87E-01	7.25E-01	8.76E-02	3.40E-01
0.500	-4.42E-02	9.81E-01	7.36E-01	9.23E-02	3.57E-01
0.750	-3.84E-02	9.67E-01	7.60E-01	9.91E-02	3.74E-01
1.000	-3.14E-02	9.33E-01	7.70E-01	1.02E-01	3.92E-01
1.500	-2.27E-02	8.83E-01	7.76E-01	1.05E-01	4.26E-01
2.000	-1.84E-02	8.57E-01	7.78E-01	1.06E-01	4.40E-01
3.000	-1.89E-02	8.59E-01	7.77E-01	1.07E-01	5.80E-01
4.000	-1.60E-02	8.30E-01	7.66E-01	1.07E-01	5.89E-01
5.000	-1.53E-02	8.26E-01	7.66E-01	1.07E-01	6.31E-01
7.500	-1.43E-02	8.15E-01	7.62E-01	1.13E-01	7.21E-01
10.000	-1.70E-02	8.22E-01	7.52E-01	1.40E-01	7.39E-01

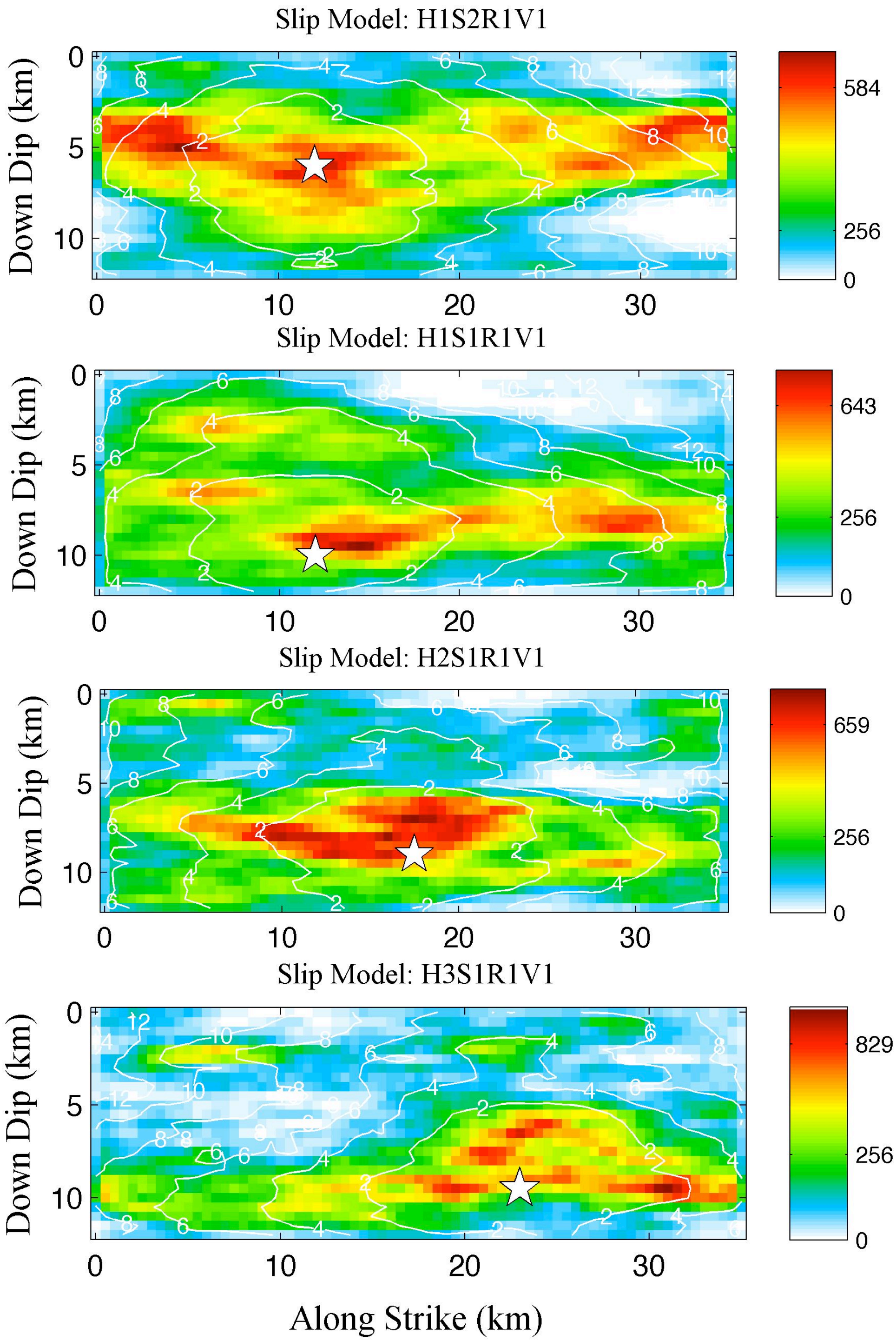

Figure 1. Examples of different slip models used for **M**7 simulations in CENA. The shaded patterns show the slip distributions over the fault plane. Contours are the rupture front and stars represent the locations of hypothetical hypocenter.

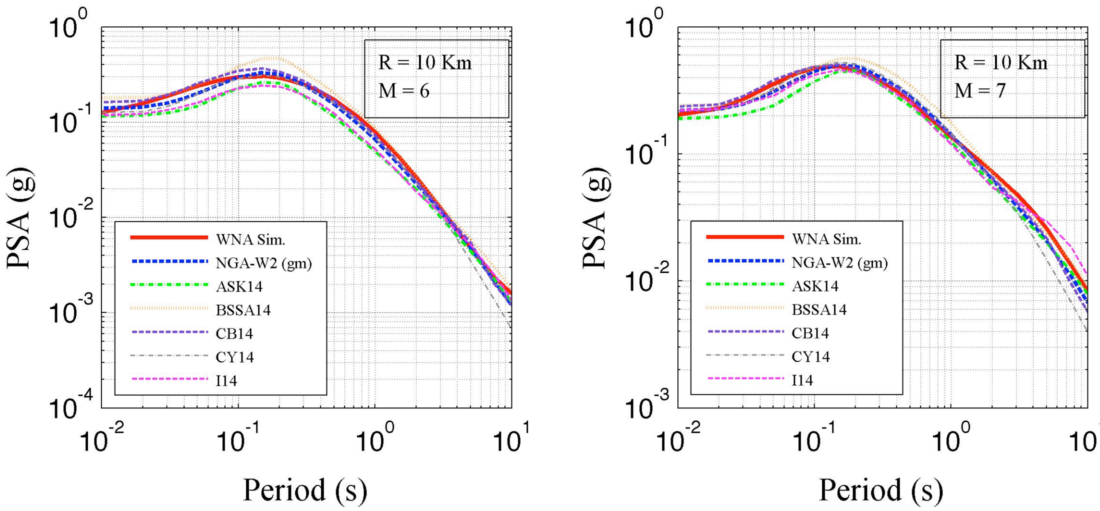

Figure 2. Comparison of spectral accelerations (5%-damped-PSA) from broadband simulations in this study and predicted values from NGA-West2 GMMs. Plots include the individual ground-motion models of ASK14, BSSA14, CB14, CY14, and I14, along with their weighted geometric mean at R_{JB} = 10 km, and for magnitudes of (left) **M**6 and (right) **M**7.

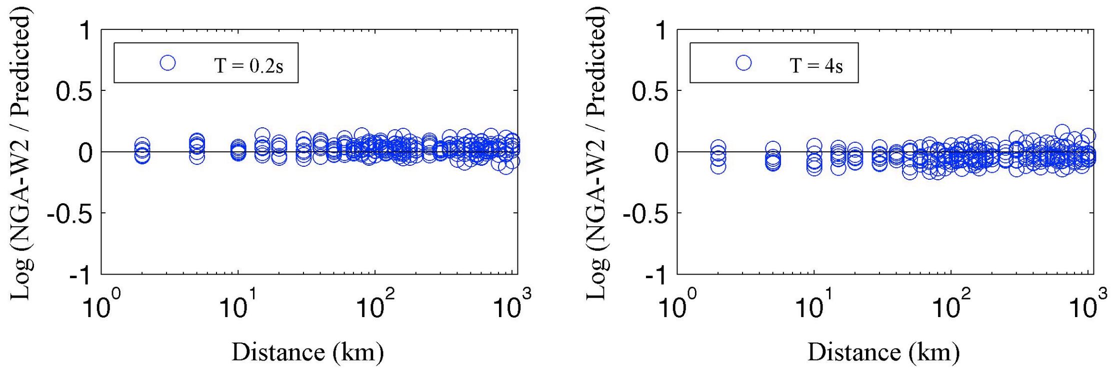

Figure 3. Examples of residuals with respect to distance from simulations in WNA. The comparison are performed with the GMMs in NGA-West2 for spectral periods of (left) T = 0.2s and (right) T = 4s.

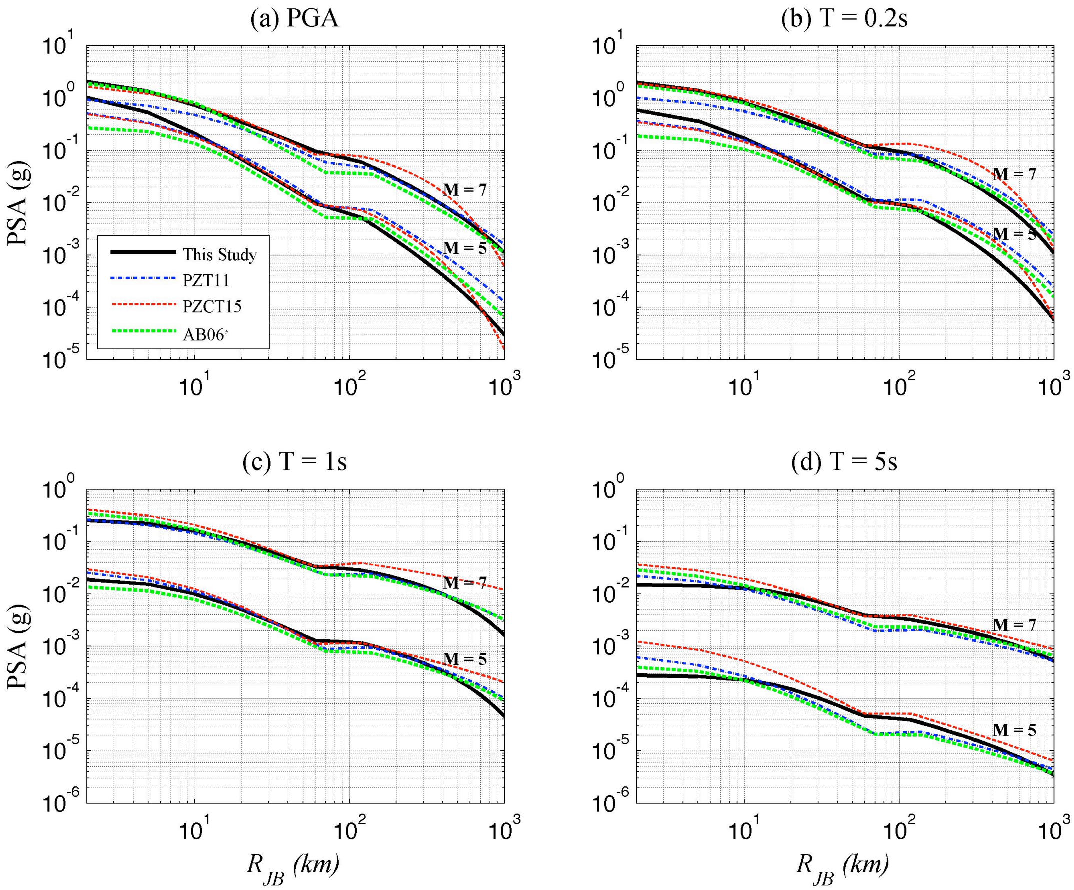

Figure 4. GMM developed in this study and comparison with AB06', PZT11, and PZCT15 ground-motion models for **M**5, and **M**7 at PGA and spectral periods of 0.2s, 1s, and 5s. Legends for (b), (c) and (d) plots are similar to the (a) plot.

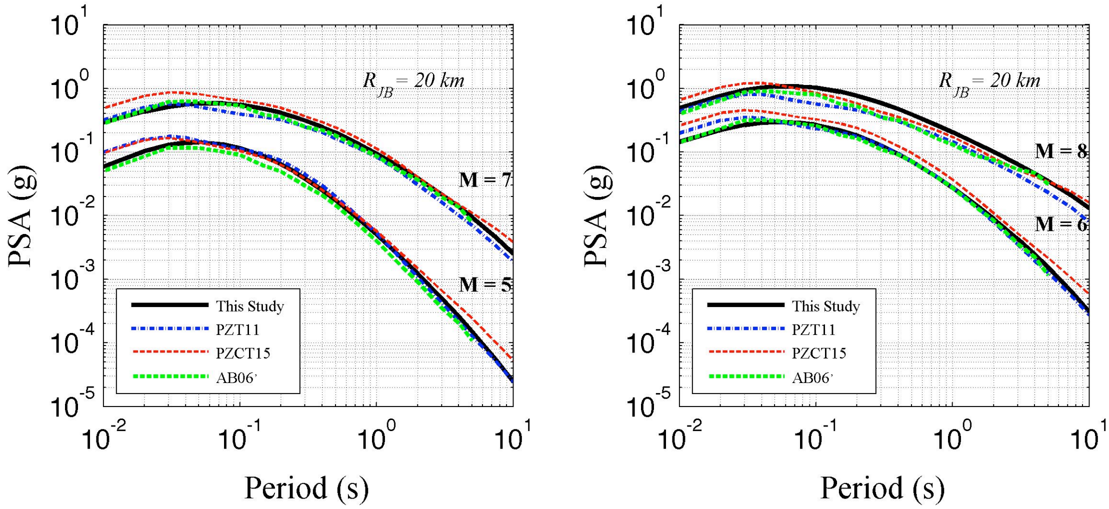

Figure 5. Comparison of the 5%-damped PSA derived from the GMM developed in this study for CENA and those obtained from AB06’, PZT11, and PZCT15 models. PSAs are shown at distance of R_{JB} = 20 km and for magnitudes of (right) **M**6 and **M**8, and (left) magnitudes of **M**5 and **M**7.

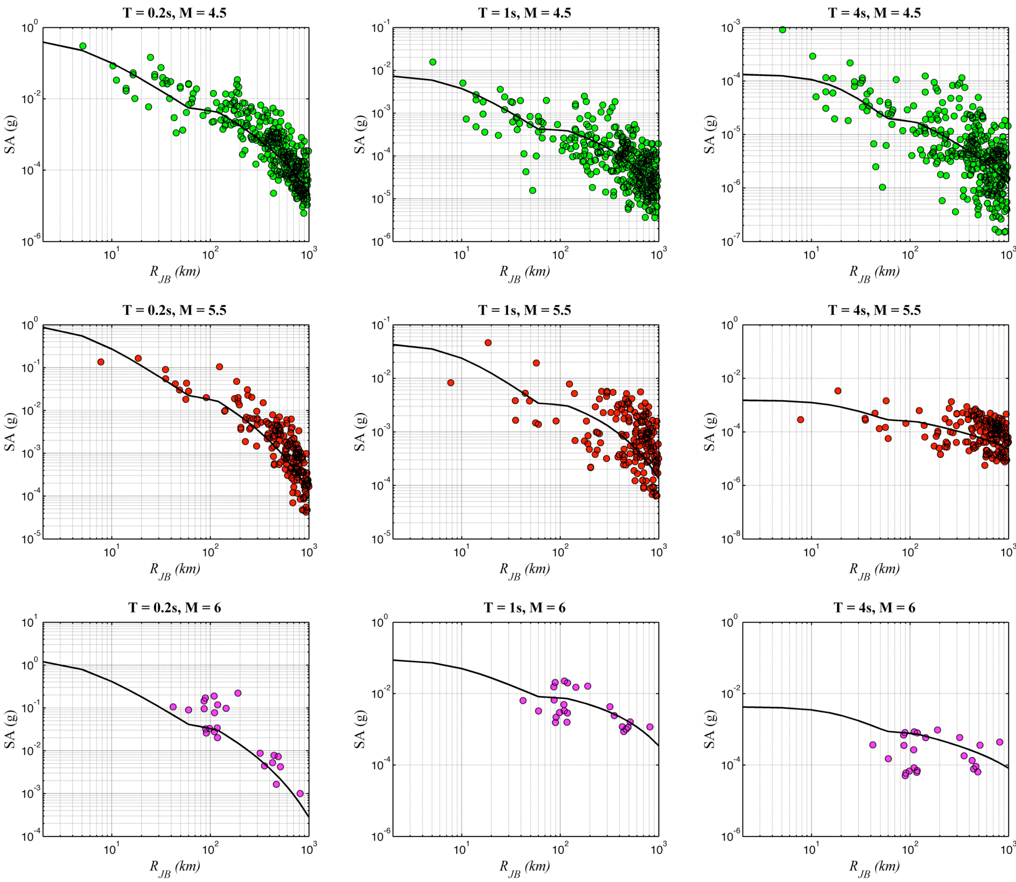

Figure 6. Comparison of the developed GMM with the recorded earthquakes available in NGA-East database for the spectral period of 0.2, 1, and 4 seconds in magnitude bins of **M**4.5, 5.5, and 6. The magnitudes represent the middle of bins of 3.75–5.25, 5.25–5.75, and 5.75–6.25 for **M**4.5, 5.5, and 6.0, respectively.

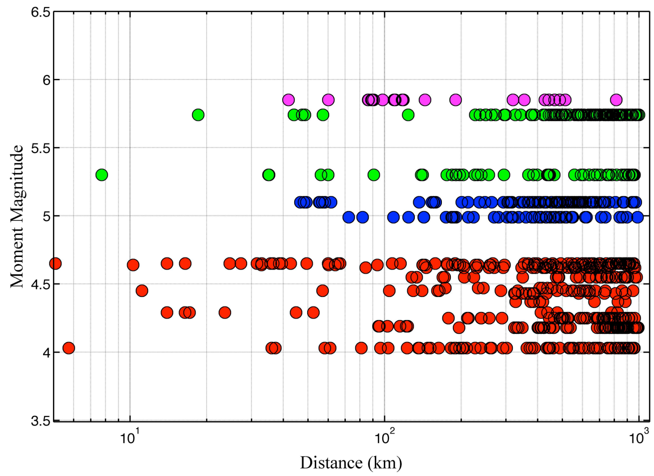

Figure 7. The magnitude and distance distribution of considered ground-motion recordings from NGA-East database.

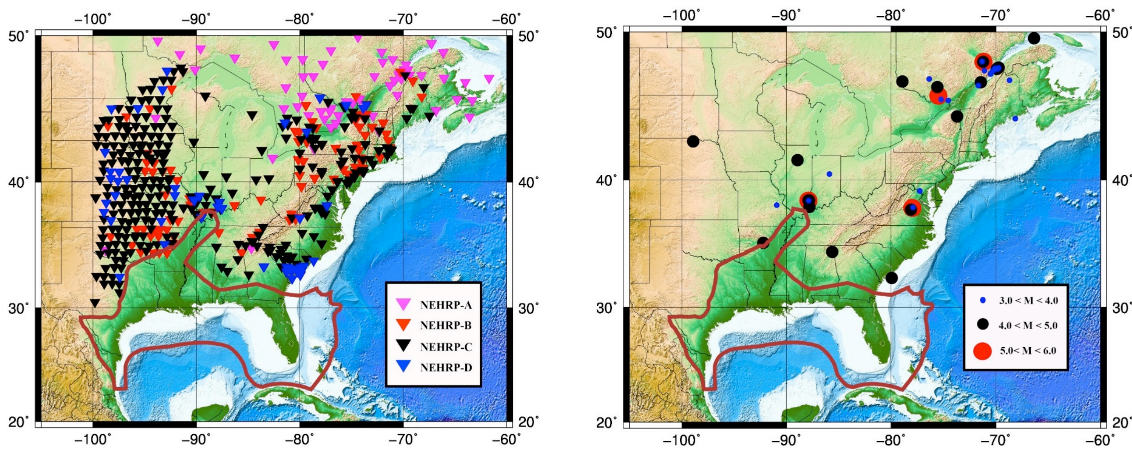

Figure 8. (Left) CENA recording stations and (right) earthquakes incorporated in the residual analyses and comparison. All stations located within Gulf Coast region and all potentially induced earthquakes (PIEs) are excluded. Stations are classified based on the NEHRP site class (Source: Pezeshk et al., 2015).

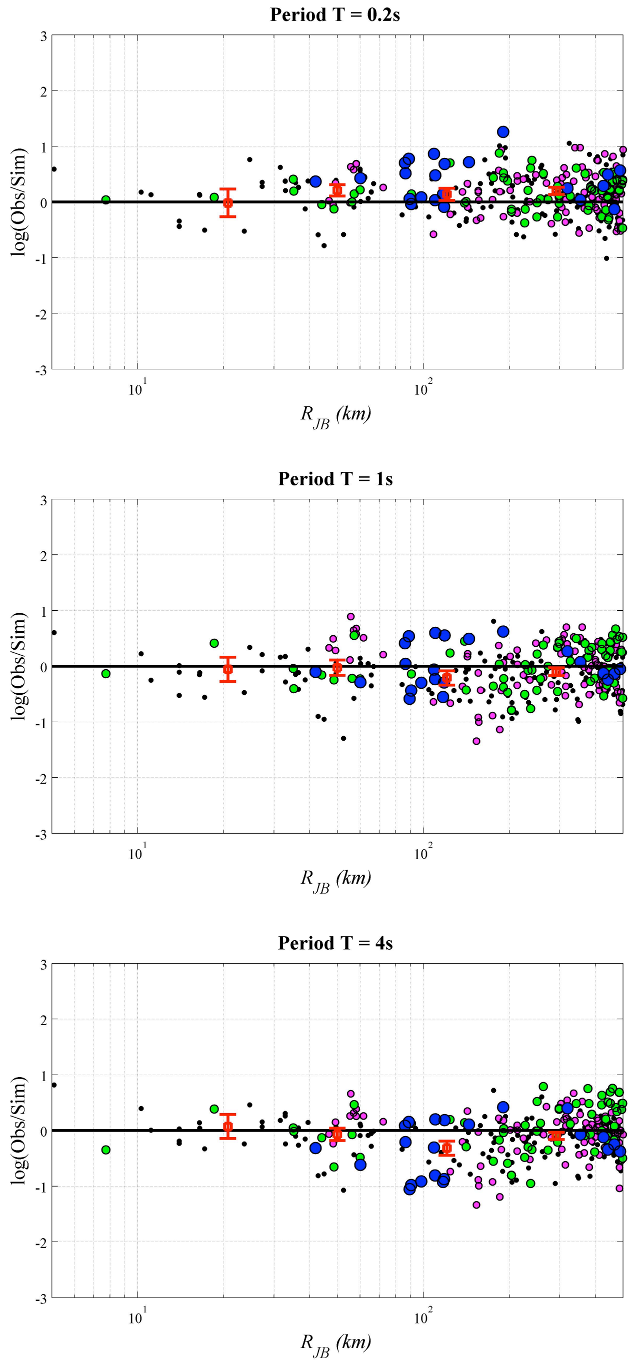

Figure 9. Residuals with respect to distance for spectral periods of T = 0.2s, 1s, and 4s. The total residuals represent the difference between observed and the predicted spectral accelerations. The size and color of each circle represents the magnitude of each event. Error bars show the 95th-percentile confidence limits of the mean (square) binned residuals.

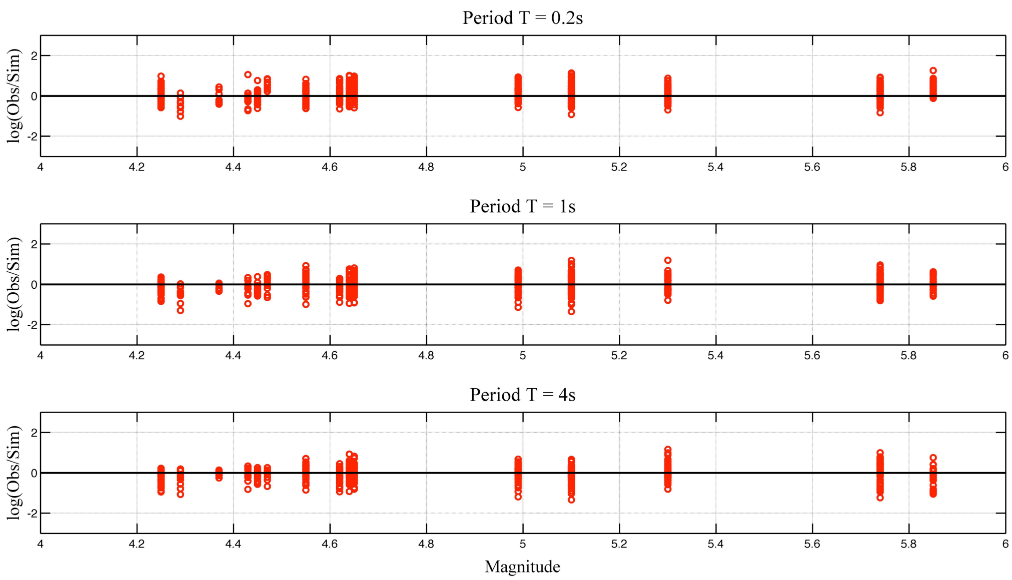

Figure 10. Residuals with respect to magnitude for the same spectral periods of T = 0.2s, 1s, and 4s that were presented in Figure 9. The total residuals represent the difference between observed and the predicted spectral accelerations.

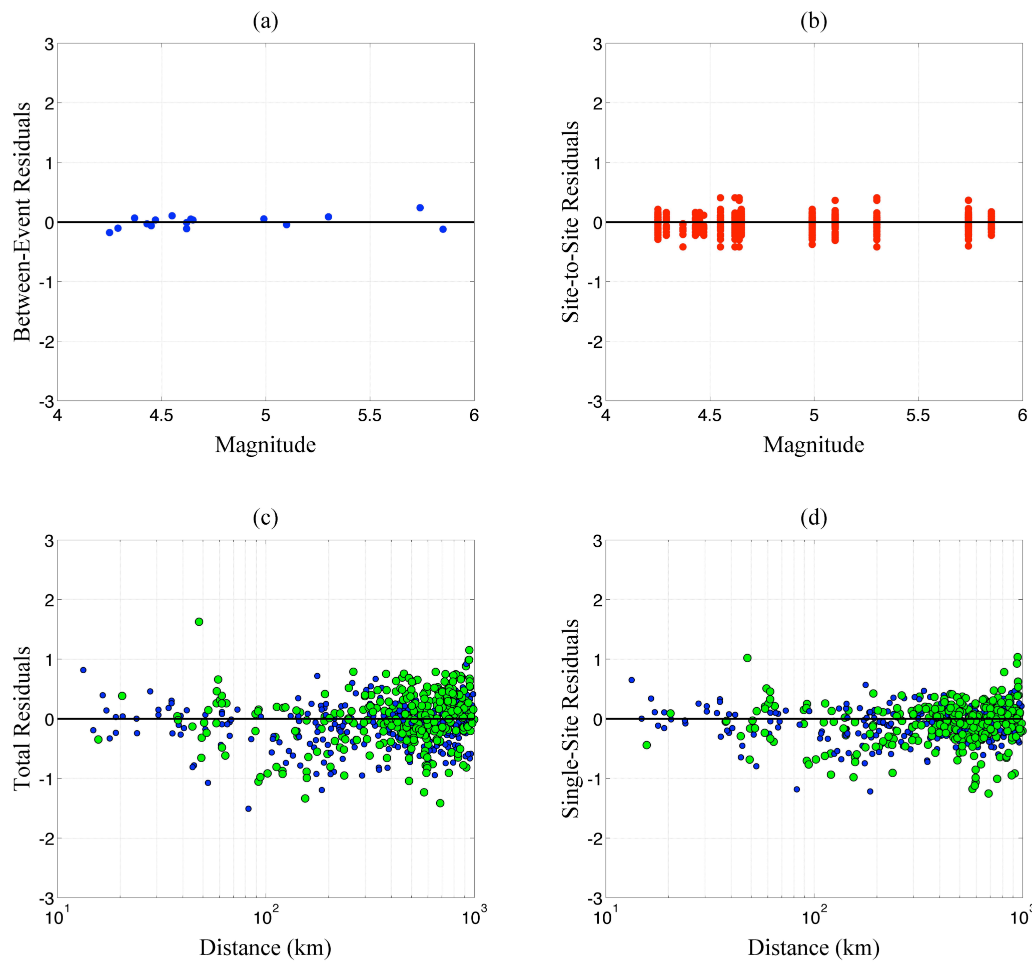

Figure 11. Residuals with respect to magnitude in terms of (a) inter-event (between-event) residuals and (b) intra-event (within-event) residuals. (c) The total residuals and (d) the single-site residuals in which local site conditions are taken into account with respect to distance.